

CRISPR-mediated activation of biosynthetic gene clusters for bioactive molecule discovery in filamentous fungi

Indra Roux¹, Clara Woodcraft¹, Jinyu Hu¹, Rebecca Wolters¹, Cameron L.M. Gilchrist¹, Yit-Heng Chooi¹

¹School of Molecular Sciences, University of Western Australia, Perth, WA 6009, Australia.

Correspondence to: yitheng.chooi@uwa.edu.au

Abstract

Accessing the full biosynthetic potential encoded in the genomes of fungi is limited by the low expression of many biosynthetic gene clusters (BGCs) under standard culture conditions. In this work, we develop a fungal CRISPR activation (CRISPRa) system for targeted upregulation of biosynthetic genes, which could accelerate the emerging genomics-driven approach to bioactive secondary metabolite discovery. We construct a fungal CRISPR/dLbCas12a-VPR system and demonstrate activation of a fluorescent reporter in *Aspergillus nidulans*. Then, we target the native nonribosomal peptide synthetase-like (NRPS-like) gene *micA* in both chromosomal and episomal contexts, achieving increases in production of the compound microperfuranone. Finally, multi-gene CRISPRa leads to the discovery of the *mic* cluster product as dehydromicroperfuranone. Additionally, we demonstrate the utility of the variant LbCas12a^{D156R}-VPR for CRISPRa at lower culture temperatures. This is the first demonstration of CRISPRa in filamentous fungi, providing a framework for CRISPR-mediated transcriptional activation of fungal BGCs.

Introduction

Fungal genome mining has emerged as a promising strategy for the discovery of novel bioactive secondary metabolites (SMs)^{1,2}. Genomic surveys have revealed that fungal species typically harbour 30–100 biosynthetic gene clusters (BGCs) each encoding the biosynthetic pathway required to produce a SM(s)³. However, the vast majority of BGCs remain uncharacterised or ‘cryptic’ as the products they encode are undetectable under standard culture conditions, often because BGCs remain ‘silent’ or lowly expressed due to tight regulatory control^{1,4}. Filamentous fungi, which have yielded a plethora of SMs with pharmaceutical and agricultural applications⁵, thus serve as attractive targets for genome mining of novel molecules.

Improved understanding of SM biosynthesis has led to the development of various bioinformatic tools and strategies for the prioritisation of BGCs for genome mining, increasing the chance of discovery of novel molecules or molecules with desired bioactivities^{6,7}. Current

strategies for activating specific BGCs typically involve promoter exchange of all individual genes in the BGC with strong promoters⁸. If a BGC contains a transcription factor (TF) gene, overexpression via promoter exchange can activate expression of the entire BGC⁹. However, in many cases this strategy requires further TF engineering¹⁰, or cluster-specific TFs are not identifiable. BGC from fungi that are genetically intractable require expression in a heterologous host⁵. Filamentous fungi are the most compatible heterologous hosts for expression of fungal BGCs, not requiring intron removal or codon optimization¹¹. For example, *Aspergillus nidulans* has been successfully utilised as a heterologous host by several groups^{12–14}, including ours^{15,16}. Whether in the native fungus or in a heterologous host, promoter exchange can be cumbersome due to the need for marker recycling¹³ for chromosomal manipulations, or the challenging episomal cloning of multiple and often large biosynthetic genes¹⁵.

To access cryptic SMs more efficiently and improve the viability of pathway-specific genome mining as an approach for drug discovery, new tools for programmable biosynthetic gene expression are necessary. Inspired by pathway-specific TFs, we aimed to develop a CRISPR activation (CRISPRa)-mediated approach for BGC activation in filamentous fungi (Fig. 1a). In CRISPRa systems, DNase-deactivated RNA-guided CRISPR/dCas ribonucleoprotein complexes linked to activation effectors are targeted to gene regulatory regions to increase gene expression^{17–19}. Taking advantage of the streamlined CRISPR RNA (crRNA) cloning and multiplexing capabilities, CRISPRa of BGCs has the potential to greatly accelerate fungal genome mining. CRISPRa has already been used to tune the expression of biosynthetic pathways^{20,21}, including in ascomycetous yeasts^{22,23}. However, to our knowledge, CRISPRa has not yet been demonstrated in filamentous fungi.

In this work, we develop a suite of fungal CRISPRa vectors based on both dLbCas12a from *Lachnospiraceae bacterium* Cas12a (previously known as Cpf1)¹⁹, and dSpCas9 from *Streptococcus pyogenes* fused to the tripartite VPR activator¹⁸, and test them in *A. nidulans*. We further explore the application of our CRISPR/dLbCas12a-VPR system for fungal BGC activation as a tool to fuel bioactive molecule discovery.

Results

Construction and testing of fungal CRISPRa systems

To develop a CRISPRa system for filamentous fungi, we constructed and tested CRISPR/dLbCas12a-VPR- and CRISPR/dSpCas9-VPR-based systems in the model organism and chassis *A. nidulans*. To evaluate alternative strategies for expressing either

dCas effector, we created parent strains with a chromosomally integrated *dCas-VPR* expression cassette and compared their performance with entirely AMA1-episomally encoded systems. The AMA1 sequence acts as an extrachromosomal vector replicator and confers increased transformation frequency in several filamentous fungi species²⁴. AMA1-bearing vectors are found at multiple copies per nucleus although their genetic stability has been reported to be limited under non-selective conditions. We built on the triple auxotrophic mutant *A. nidulans* LO8030²⁵, which can maintain AMA1 vectors by complementation with the selectable markers *pyrG*, *riboB*, *pyroA*¹⁵. The modular nature of the AMA1 vector set allowed rapid building, testing and exchange of the different CRISPRa components. For an initial proof-of-concept, we built as test target a fluorescent reporter fusing *mCherry* to *Parastagonospora nodorum elcA* promoter (P_{elcA}), which belongs to a ‘silent’ polyketide synthase gene²⁶, and delivered it encoded on a AMA1 vector.

Cas12a systems have the potential to simplify multiplexing due to their short crRNA and their capability to process the precursor crRNA array²⁷. Furthermore, crRNAs can be excised from RNA polymerase II (RNAPII)-driven transcripts²⁸ allowing us to build a crRNA expression cassette with *gpdA* promoter (P_{gpdA}) and *trpC* terminator (T_{trpC}) (Supplementary note 1), which are parts widely portable across fungal species²⁹. We tested the CRISPRa system targeting P_{elcA} with a four-crRNA array encoded on an AMA1-pyroA vector. Due to the lack of characterization of the transcription start site (TSS) of the *elcA* gene, we targeted the crRNAs to a window 88–327bp upstream of the open reading frame start codon (Fig. 1b). After growing mycelial mass, we observed activation of *mCherry* expression in the CRISPRa transformants (Fig. 1b, Supplementary Fig. 1) compared to the no crRNA control, in both chromosomally and episomally expressed dLbCas12a-VPR systems (Fig. 1b). The results demonstrated the viability of the RNAPII-promoter P_{gpdA} to deliver LbCas12a crRNA arrays.

In parallel, we built and tested a dSpCas9-VPR system, with a sgRNA expression cassette driven by the RNA polymerase III promoter U3 from *Aspergillus fumigatus* (AfP_{U3})³⁰ (Supplementary note 1). In this case, four sgRNA were tested individually, targeting a window 162–342 bp from the reporter start codon, and delivered in a single AMA1-pyrG vector together with the reporter construct P_{elcA} -*mCherry*. We observed that the system with chromosomal expression of *dSpCas9-VPR* resulted in activation levels only noticeable at prolonged exposure times, while the system with episomally expressed dSpCas9-VPR resulted in stronger fluorescence (Fig. 1c, Supplementary Fig. 2a and b). A possible interpretation is that the single-copy chromosomal *dSpCas9-VPR* cassette failed to achieve expression levels above the required threshold for strong observable activity, making the multicopy AMA1-encoded system more effective in comparison. We also observed a sgRNA-dependent variation in the activation intensity (Supplementary Fig. 2b). We further attempted

to deliver sgRNAs from an independent AMA1-pyruA vector, but when co-transformed with the reporter vector and the dSpCas9-VPR expression vector, fluorescence was not observed (Supplementary Fig. 2c).

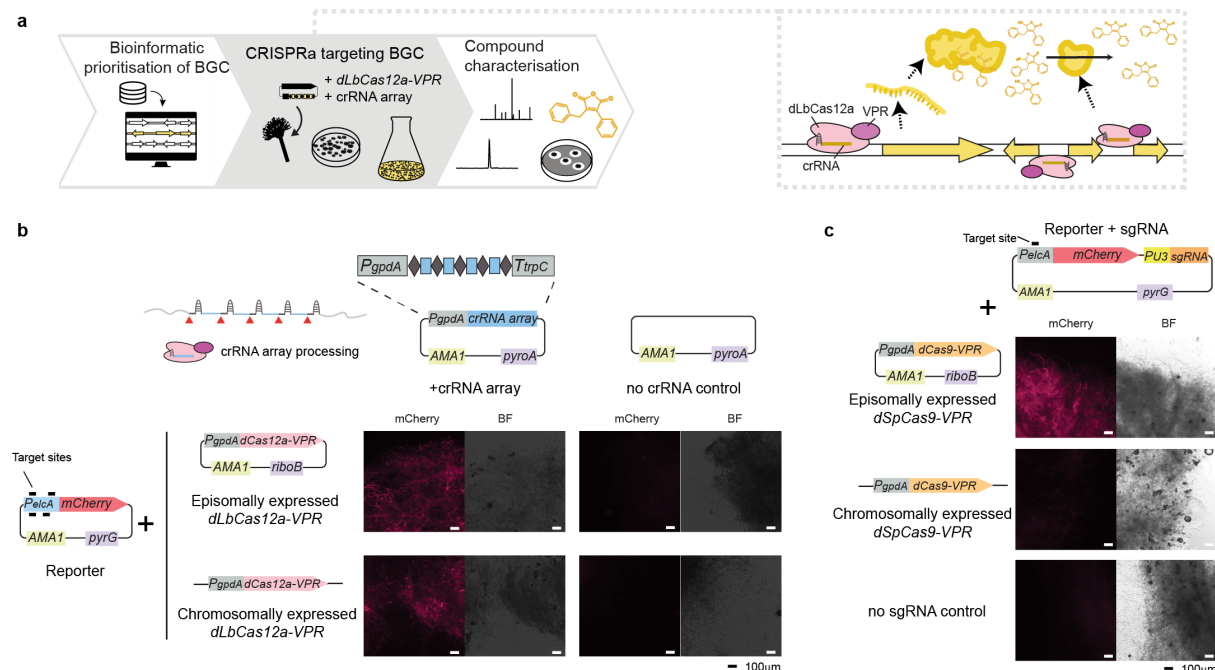


Fig. 1 Proof-of-concept for fungal CRISPRa **a**. Schematic of a CRISPRa-based genome mining pipeline. After BGC bioinformatic prioritisation, the designed crRNAs are rapidly assembled in an expression vector and transformed into the fungal host along with the dCas effector. The CRISPRa complex is targeted to the regulatory regions of the selected BGC, upregulating gene expression and consequently increasing production of the encoded compound(s). This would facilitate compound detection, screening for bioactivity and further chemical characterisation. **b**. CRISPR/dCas12a-VPR mediated activation of *P_{elcA}-mCherry* in *A. nidulans*. Representative fluorescent microscopy images of CRISPRa transformant mycelia demonstrate consistent *mCherry* reporter activation, which implies the processing of crRNA array from a *P_{gpdA}*-derived RNAPII-driven transcript by dLbCas12a-VPR. Activation is observed both episomally and chromosomally encoded dLbCas12a-VPR systems (Supplementary Fig. 1). **c**. Activation strength of the CRISPR/dSpCas9-VPR system showed dependency on dSpCas9-VPR expression strategy (Supplementary Fig. 2). In all microscopy images mycelia were observed under brightfield (BF) and mCherry filter after overnight growth on stationary liquid culture at 37 °C. Scale bar 100 µm.

Activating *micA* for increased microperfurane production

As CRISPR/dLbCas12a-VPR demonstrated better versatility in our initial tests, we decided to proceed to the next phase with this system. To test whether CRISPR/dLbCas12a-VPR mediated activation of fungal biosynthetic genes could induce metabolite production, we targeted the native *A. nidulans micA* (AN3396) gene which encodes a nonribosomal peptide synthetase-like (NRPS-like) enzyme responsible for the biosynthesis of microperfurane (**1**) (Fig. 2a). The biosynthetic function of *micA* had been previously decoded by Yeh et al.³¹,

following a promoter replacement strategy, after unsuccessful attempts to elicit the biosynthesis of cryptic NRPS-like products by varying *A. nidulans* culture conditions.

Based on available *A. nidulans* TSS annotation^{32,33}, we followed previously devised guidelines for CRISPRa in eukaryotes³⁴ and targeted a region 119–303 bp upstream of the TSS with a four-crRNA array named MU (*micA* Upstream TSS) (Fig. 2b). To explore the utility of CRISPRa for genes that lack TSS information, which is the case for 59% of *A. nidulans* BGC genes (Supplementary Fig. 3a), we also tested an alternative TSS annotation-blind targeting criteria, taking the gene start codon as reference. Given that most *A. nidulans* BGC genes have short 5' untranslated region (UTR) (Supplementary Fig. 3b), we targeted a window 139–324 bp upstream of the *micA* start codon with a four-crRNA named MD (*micA* Downstream TSS), which in this case corresponds to the 5' UTR of *micA*. Analysis by liquid chromatography coupled to a diode array detector and mass spectrometer (LC-DAD-MS) showed increases in the production of **1** in media extracts from all CRISPRa transformants when compared to the background levels in the controls (Fig. 2c). Interestingly, targeting the 5' UTR of *micA* with crRNA array MD resulted in significantly higher production than when targeting the *micA* promoter region with crRNA array MU, with titres of **1** up to 0.6 mg L⁻¹ (Fig. 2d). Nevertheless, targeting with MU still led to a ~4.5-fold increase in production with a titre up to 0.2 mg L⁻¹ compared to the controls. No significant difference in performance was observed when comparing between chromosomally and episomally expressed dLbCas12a-VPR systems for both crRNA arrays.

In order to enable rapid cloning of different crRNAs for further testing, we established a domesticated version of the AMA1-pyroA expression vector, which allowed one-step Type IIS cloning of crRNA arrays using annealed oligonucleotides (Supplementary Fig. 4). We verified the null effect of P_{gpdA} promoter domestication (Supplementary Fig. 4b).

To examine the effect of each crRNA in *micA* activation, individual crRNAs from MD and MU arrays were delivered in strains harbouring chromosomally integrated *dLbCas12a-VPR* (Fig. 2e and Supplementary Fig. 5). We observed a minimal increase in the production of **1** when targeting with some MD crRNA, while in most cases the production of **1** was indistinguishable from the no crRNA control. The broad difference between the production of **1** in strains with single crRNAs and the observed with multiple-crRNA array CRISPRa is indicative of a synergistic activation effect (Fig. 2e).

To test whether the production of **1** could be further increased, we targeted *micA* with both MD and MU crRNA arrays simultaneously. To this end, we re-cloned the crRNA array MD into an AMA1-pyrG vector to allow co-transformation with the crRNA array MU encoded on an AMA1-pyroA vector. Co-transformation of both MD and MU crRNA arrays for *micA* activation

resulted in further increase in the production of **1** (up to $\sim 0.8 \text{ mg L}^{-1}$) (Supplementary Fig. 6). Interestingly, the crRNA array MD alone delivered from the AMA1-pyrG vector resulted in a considerable increase in the titre of **1** compared to when delivered using AMA1-pyrG vector, which might contribute to the dual crRNA array increased production (Supplementary Fig. 6). Finally, to evaluate the broader utility of CRISPRa targeting episomal genes in *A. nidulans*, we co-transformed additional copies of *micA* encoded on an AMA1 vector. The transformants harbouring episomal copies of *micA* with its full-length promoter showed relatively high basal production of **1** even in the absence of CRISPRa (Fig. 2f). However, we still observed a consistent increase in the titres of **1** when CRISPRa of *micA* was performed with either MD or MU crRNA arrays, reaching up to over 4 mg L^{-1} (Fig. 2f). We further tested targeting a shorter episomal *micA* variant with low basal production of **1**. When co-transforming with MD, targeting the still-present 5' UTR, we observed the largest activation fold change with a ~ 30 -fold increase in the production of **1** compared to the control, reaching final titres of $\sim 1.5 \text{ mg L}^{-1}$ (Fig. 2g). Taken together, these results show that CRISPRa can affect the expression of episomally encoded genes, as the increase in the production of **1** is not explained by the activation of chromosomal *micA* alone.

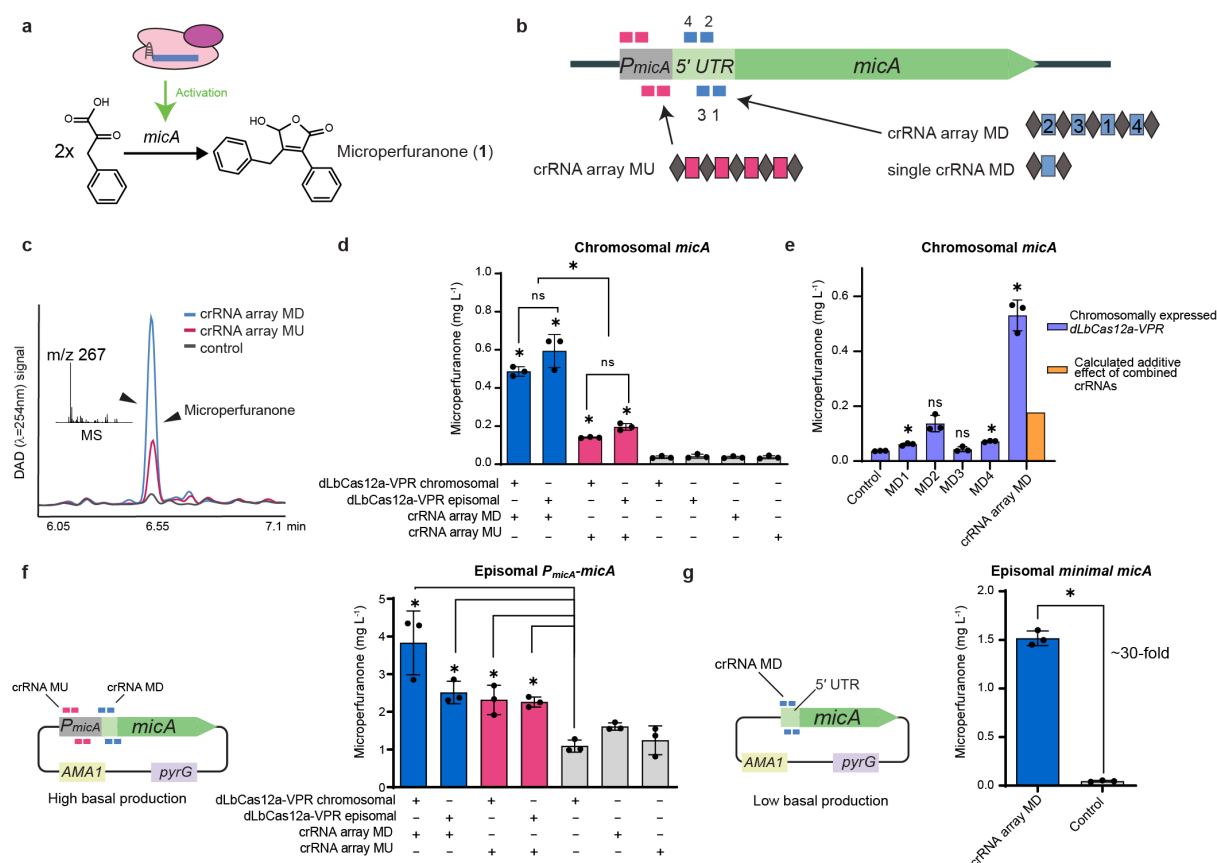


Fig. 2 . CRISPRa-mediated microperfurane (1**) production. a.** Upregulation of *micA* results in the biosynthesis of **1** from two phenylpyruvate³¹. **b.** Chromosomal *micA* gene with individual crRNA binding sites shown in magenta (crRNA array MU) and blue (crRNA array MD).

Numbers assigned to MD crRNAs are indicative of targeting position in respect to *micA* start codon, with their position in the crRNA array MD also indicated in the scheme. **c.** DAD ($\lambda=254$ nm) chromatograms of *A. nidulans* culture media extracts show increases in the peak identified as **1** in strains with CRISPR-mediated activation of *micA* (magenta and blue) as compared to the control with no crRNA (grey). Expected mass of **1** is observed as main ion in the peak by MS. **d.** CRISPR-mediated activation of chromosomal *micA*. All CRISPRa strains showed a significant increase in the production of **1** compared to their respective dLbCas12a-VPR control with no crRNA. Targeting CRISPRa with MD crRNA array (blue) resulted in significantly higher production of **1** compared to targeting with MU crRNA (magenta). There was no significant difference between both dLbCas12a-VPR expression strategies. **e.** When targeting *micA* with single MD crRNAs low or no activation is observed compared to the no crRNA control. The low calculated additive of single crRNA CRISPRa (described in Methods) suggests a synergistic activation effect when making use of the four-crRNA array MD. **f.** Increases in the titre of **1** are observed in media extracts of CRISPRa strains with extra episomal *micA* copies (high basal production) compared to the no crRNA control in strains with episomal *micA* vector. **g.** In strains harbouring episomal copies of a shorter *micA* variant (low basal production), CRISPRa increased the production of **1** by ~30-fold compared to the control. In all the figures, calculated titre (mg L⁻¹) values are the mean of three biological replicates which specific values are indicated as black dots, error bars represent SD. Two-sided Welch's T-test with Holm-Šidák multiplicity correction per figure was performed. Asterisk indicates corrected P-value<0.05, (ns) not significant. Individual P-values are listed in Supplementary Table 9.

Multi-gene activation uncovered cryptic gene cluster product

The gene *micA* (AN3396) has been proposed to belong to a BGC, which also contains a putative cytochrome P450 (AN3394) and an hypothetical gene (AN3395)^{31,35}, henceforth referred to as *micB* and *micC*, respectively. However, the final product of the *mic* cluster has remained uncharacterised.

To assess the feasibility of performing simultaneous activation of multiple genes with CRISPR/dLbCas12a-VPR, we aimed to co-activate the proposed *mic* cluster. We co-transformed the four-crRNA array MD targeting *micA* along with a second crRNA array targeting *micB* and *micC* (Fig. 3a). This new three-crRNA array, named crRNA array P, targeted a window of 209bp in the middle of the short 396 bp bi-directional promoter between the divergently oriented *micB* and *micC* genes. We delivered the two crRNA arrays from independent AMA1 episomal vectors in strains harbouring chromosomally integrated dLbCas12a-VPR (Fig. 3a). To account for the above-mentioned influence of the crRNA delivery vector selection marker on CRISPRa strength, we tested both dual plasmid delivery combinations with *pyrG* and *pyroA* selection markers (Fig. 3a).

LC-DAD-MS analysis of *A. nidulans* culture extracts showed that both multiplexed-CRISPRa strains presented a decrease in the precursor microperfuraneone (**1**) and an increase in the production of three new peaks detected by DAD and MS, arbitrarily named peaks I, II and III (Fig. 3c, Supplementary Fig. 7a–b). However, the magnitude of the changes in the metabolic

profile was dependent on the marker combination used in the delivery of the crRNA arrays. Given that the precursor **1** does not appear to be limiting as it remains present under all configurations, crRNA array P delivery on an AMA1-pyrG vector favoured the production of the peaks I–III compared to when delivered on AMA1-pyroA (Fig. 3d). We further tested the best performer crRNA array delivery combination switching to episomally encoded *dLbCas12a-VPR* and observed an increased production of the peaks I–III relative to the peak from **1** (Fig. 3d, Supplementary Fig. 7c). Taken together these results indicate that multiple gene CRISPRa can be used to explore the metabolite products of a cryptic BGC and that the activity can be tuned to favour the final product of the cluster.

The observed mass of the ions accumulated in the peaks I–III was m/z 265 $[M+H]^+$, 2 Da less than the molecular mass of **1**, suggesting that an oxidation has occurred. Searching the chemical literature for structures related to **1** corresponding to a mass of 264 Da led us to a previously reported metabolite, 3-carboxy-2,4-diphenyl-but-2-enoic anhydride, herein renamed as dehydromicroperfurane (**2**) (Fig. 3b) first isolated from *A. nidulans* IFO 6398 as a plant growth promoting compound³⁶. We further analysed the CRISPRa strain crude extract by LC-MS/MS and observed that the fragmentation pattern of the 265 m/z ions shared almost all masses with the predicted spectra for **2** by CFM-ID³⁷ (Supplementary Table 1).

To ensure that the production of the peaks I–III is due to CRISPRa co-targeting the *micB–C* promoter, we further verified the final product of the *mic* cluster by promoter replacement of *micA*, *micB* and *micC*. When expressing *micA* and *micB* from alcohol inducible promoters, the metabolic profile presented the peaks I–III as observed by CRISPRa, although the metabolites were produced in higher quantities (Supplementary Fig. 8a). The co-expression of *micA–C* resulted in the same metabolic profile as *micA–B* (Supplementary Fig. 8a). This revealed the function of MicB as a cytochrome P450 monooxygenase responsible for converting a secondary alcohol on **1** to a ketone group, forming a maleic acid anhydride moiety.

To corroborate the structure of the compounds, we attempted to purify the peaks I–III. The peaks I–II co-eluted during semi-preparative HPLC purification, while peak III could be isolated as a single peak. Surprisingly, the ¹H-NMR and ¹³C-NMR spectra of the peaks I–II mixture and peak III in deuterated chloroform appear to be identical (Supplementary Table 2 and Supplementary Fig. 9–12), and both matched the previously reported chemical shifts for **2**³⁶. When reconstituting the NMR sample in methanol for analysis by LC-DAD-MS, the purified peaks reverted to multiple peaks (Supplementary Fig. 8c) and we further observed that the samples also exist as mixtures when analysed by NMR in deuterated methanol (Supplementary Fig. 13–14). These results suggest that the compounds in the peaks I–III are interchangeable tautomeric or opened/closed ring forms in acetonitrile or methanol

(Supplementary Fig. 8d) but existed as a single entity in chloroform during NMR analysis (Supplementary Table 2). Taken together, the results from LC-MS/MS and NMR analysis supported that the metabolite product of the *mic* cluster as **2**.

Due to increased polarity, **2** was only extractable from the culture medium with acidified ethyl acetate or adsorbent resin (Supplementary Fig. 8b), which might explain why this compound has not been observed in previous studies where ethyl acetate extraction was used for metabolite profiling of *A. nidulans*^{31,38}.

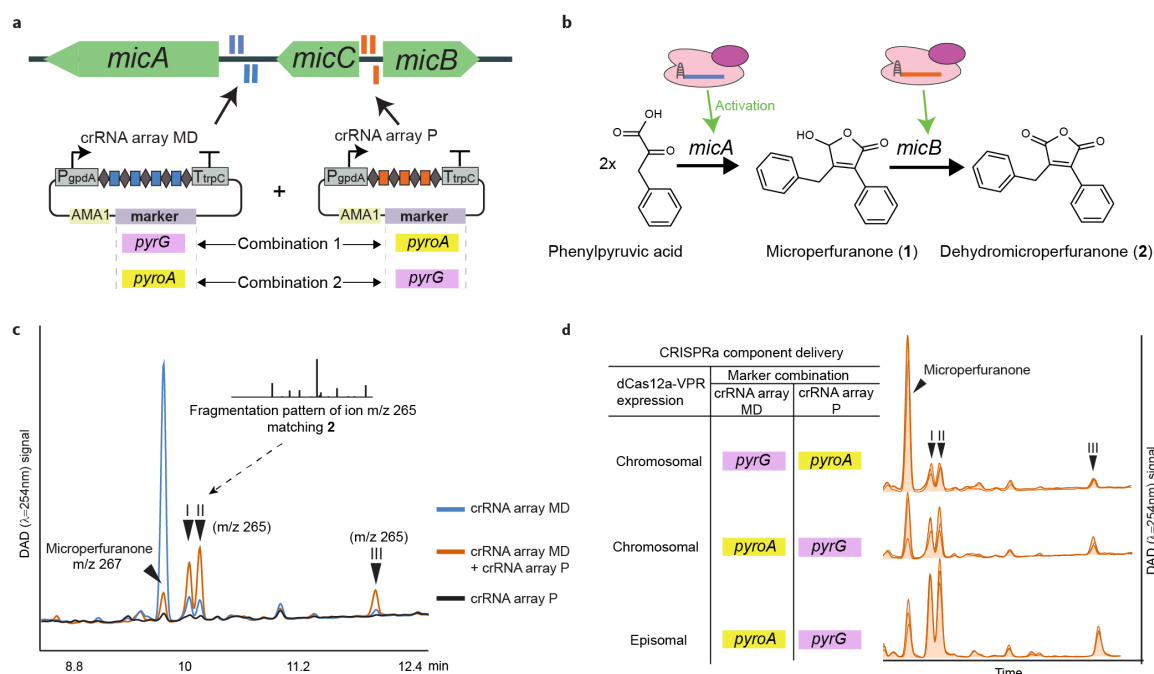


Fig. 3. Elucidating the *mic* cluster final product with multi-gene activation **a**. Schematic of the experimental set-up of *mic* cluster activation with two-vector crRNA arrays delivery and different markers combinations of *pyrG* (purple) and *pyroA* (yellow). The *mic* cluster genes are shown in green alongside the target sites of crRNA MD array (blue) and crRNA P array (orange). **b**. Proposed dehydromicroperfurane (**2**) structure and biosynthetic pathway. **c**. Representative overlaid DAD ($\lambda=254$ nm) chromatograms of media extracts from strains with both crRNA arrays MD and P (orange), crRNA array MD (blue) and crRNA array P (black). Multi-gene CRISPRa results in the increase of the peaks I–III whose main ion m/z 265 yielded a fragmentation pattern matching **2** by LC-MS/MS analysis (Supplementary Table 1). **d**. Production of each peak in multiple activation strains is dependent on CRISPRa component delivery strategy. The different DAD ($\lambda=254$ nm) chromatograms represent three biological replicates per delivery strategy (Supplementary Fig. 7). We observe that the production of the peaks I–III is favoured in the marker combination crRNA MD in an AMA1-*pyroA* vector and crRNA P in an AMA1-*pyrG* vector.

dLbCas12a^{D156R} improves activation at lower temperatures

The activity of Cas12a systems is modulated by temperature³⁹. This could compromise the applicability of fungal CRISPRa, as the majority of fungi have optimum growth temperatures between 25 °C and 30 °C⁴⁰ and the production of some SMs is favoured at lower

temperatures¹. To evaluate CRISPRa performance at lower temperatures, we observed CRISPR/dSpCas9-VPR and CRISPR/dLbCas12a-VPR mediated activation of the *P_{elcA}-mCherry* reporter across multiple temperatures. The fluorescence observed at 30 °C was comparable to the samples grown at 37 °C in both systems, but at 25 °C only observable in CRISPR/dSpCas9-VPR samples although at lower intensity (Supplementary Fig. 15).

Due to the restrictions on dLbCas12a-VPR activity at 25 °C a putative temperature tolerant variant was investigated. Taking inspiration from the AsCas12a^{E174R} variant, recently reported to possess increased double stranded DNA cleavage efficiency *in vitro* at 25 °C⁴¹, we built an LbCas12a mutant harbouring the homologous mutation D156R identified by aligning the AsCas12a/LbCas12a crystal structures^{42,43} (Supplementary Fig. 16).

We tested the variant dLbCas12a^{D156R}-VPR targeting chromosomal *micA* with the crRNA array MD. We observed significant CRISPR/dLbCas12a^{D156R}-VPR mediated activation at 25 °C, a temperature at which CRISPR/dLbCas12a mediated activation was not observed (Fig. 4b). However, at 37 °C CRISPR/dLbCas12a^{D156R}-VPR achieved lower final production of **1** than the original dLbCas12a-VPR system (Fig. 4b). We also observed evidence of CRISPR/dLbCas12a^{D156R}-VPR mediated fluorescence activation at 25 °C (Fig. 4a, Supplementary Fig. 15).

The presence of protospacer adjacent motif (PAM) near the target is a critical requirement for CRISPR systems, in the case of LbCas12a systems the sequence TTTV⁴⁴. The variant LbCas12a^{D156R} has been reported to exhibit improved recognition of the non-canonical PAM sequence TTCN⁴⁵. We tested a poly-crRNA array targeting TTCN PAM sites in the 5' UTR of *micA*, and observed an improved activation mediated by the dLbCas12a^{D156R} variant over the original dLbCas12a system at 37 °C (Fig. 4b). In most *A. nidulans* BGC genes around 10 canonical TTTV PAM sites can be found in a targetable window for activation (Supplementary Fig. 17). Nevertheless, targeting TTCN can be considered if PAM site availability is a limiting factor.

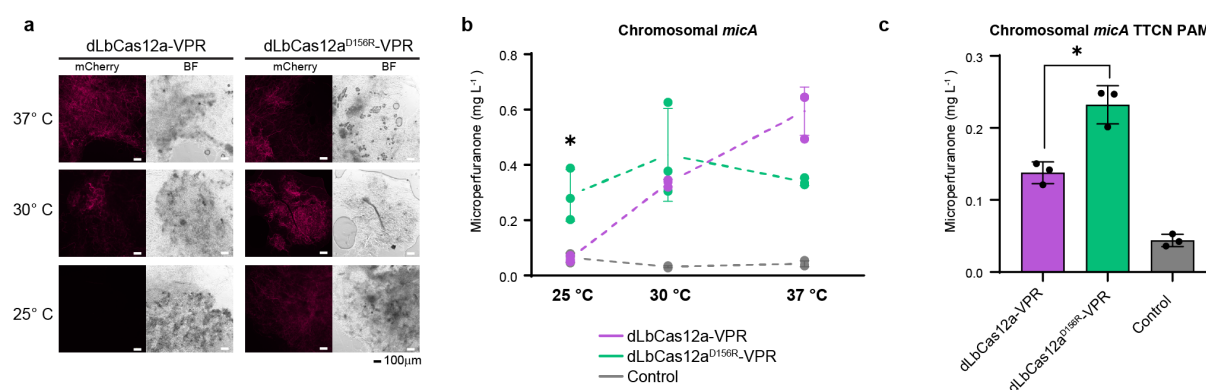


Fig. 4. The variant dLbCas12a^{D156R}-VPR outperforms at some limiting conditions for dLbCas12a-VPR. **a.** Representative microscopy images of *A. nidulans* mycelia grown at different temperatures show that CRISPR/dLbCas12a-VPR mediated activation of the fluorescent reporter *P_{elcA}-mCherry* is restricted at 25 °C. The variant dLbCas12a^{D156R}-VPR presents observable fluorescence at 25 °C unlike the original system (Supplementary Fig. 15). In all microscopy images mycelia were observed under brightfield (BF) and mCherry filter. Scale bar 100 μm. **b.** *A. nidulans* growth temperature of 25°C is limiting for CRISPR/dLbCas12a-VPR mediated *micA* activation (purple), as no increments in microperfuraneone (**1**) are observed. The variant dLbCas12a^{D156R}-VPR (green) demonstrated CRISPRa activity at 25°C, achieving a ~4.5-fold increase in the production of **1** compared to the no crRNA control. However, the activity of dLbCas12a^{D156R}-VPR was limited compared to the original dLbCas12a-VPR system at 37 °C. **c.** Activity at the alternative PAM site TTCN is increased by the dLbCas12a^{D156R}-VPR variant. In all figures, calculated titre (mg L⁻¹) values are the mean of three biological replicates whose specific values are indicated as dots, error bars represent SD. Two-sided Welch's T-test with was performed. Asterisk indicates corrected P-value<0.05. Individual P-values are listed in Supplementary Table 9.

Discussion

In this work, we reported the first application of CRISPRa in an ascomycetous filamentous fungus belonging to the Pezizomycotina taxon, known to harbour diverse BGCs. We first tested different strategies for expressing both CRISPR/dSpCas9-VPR and CRISPR/dLbCas12a-VPR system components in *A. nidulans*, observing the activation of a fluorescent reporter. We then demonstrated the feasibility of CRISPR/dLbCas12a-VPR mediated activation of *A. nidulans* native biosynthetic genes to induce SM production. This led to the rediscovery of dehydromicroperfuraneone, in which the molecule was associated with the *mic* cluster for the first time. Additionally, we demonstrated CRISPRa-mediated upregulation of genes in episomal constructs, which could be a valuable tool to activate BGCs from diverse fungi captured on vectors and heterologously expressed in *A. nidulans* as a chassis^{12,15}.

The CRISPR/dLbCas12a-VPR system presented advantages in multiplexing capability and supported expression of CRISPRa components in various configurations. Additionally, as Cas12a successfully processed transcripts driven by the RNAPII promoter *P_{gpdA}*, it allowed us to build an AMA1-derived CRISPRa vector set with common fungal genetic parts, increasing the potential portability of the CRISPRa system across fungal species. We targeted *micA* with multiple crRNAs to increase the likelihood of achieving strong activation, an approach used in pooled CRISPRa screenings⁴⁶, and observed a synergistic activation effect. Cas12a has been demonstrated to process up to 25 crRNAs from a single transcript in the literature⁴⁷, indicating that CRISPR/dCas12a systems may have the potential to extend multiplexing to target whole BGCs from a single crRNA array in future works. Additionally, next generation activators⁴⁸ could improve dCas12a-based CRISPRa activation strength.

We also explored the viability of selecting crRNA targets in a TSS annotation-blind manner, considering filamentous fungi genomes in public databases often lack 5' UTR annotations. In the case of *micA*, targeting a short distance upstream of the gene start codon, despite falling in the 5'UTR, resulted in successful production of microperforanone. This is surprising, as it contradicts the possible roadblock of transcription effect²², and might imply that the binding of dLbCas12a-VPRs to *micA* 5' UTR region redefines the local transcriptional landscape by other means⁴⁹. Although this might be a locus-specific effect, exploring TSS annotation-blind criteria could be a viable alternative when targeting BGCs with incomplete gene annotation, as demonstrated for *P_{elcA}* and *micA*.

Considering the potential limitation of dLbCas12a-VPR in filamentous fungi with low optimal growth temperatures, we built and tested dLbCas12a^{D156R}-VPR. During the preparation of this manuscript, the LbCas12a^{D156R} variant was reported to exhibit increased low-temperature genome editing efficiency *in vivo*⁵⁰. Here, we demonstrated that the temperature tolerance property is translatable to CRISPRa, allowing activity at limiting temperatures for the original system.

In conclusion, we believe this work represents a valuable expansion to the fungal CRISPR toolbox and provides a foundation for the further development of CRISPR-based transcriptional activators as a tool for the discovery of novel fungal SMs. The CRISPRa vector set could also contribute to SM discovery by targeting different combinations of genes and aiding the elucidation of the resulting SM intermediates, interrogating BGC regulation with specific epigenetic effectors as well as interrogation of other related biological functions.

Methods

Plasmids Construction

Main vectors for the Cas12a systems will be deposited in Addgene. All vectors are listed along with their description and the cloning method used in Supplementary Table 4. Plasmids were generated using one of the following methods: restriction enzyme cloning with PacI, NotI and T4 DNA ligase; Type IIS assembly with BsmBI and annealed oligo cloning; yeast homologous recombination or isothermal assembly with NEBuilder HiFi DNA Assembly Master Mix (NEB). All primers used are listed in Supplementary Table 8 along with their destination construct and source of DNA template. The AMA1 fungal vector pKW20088⁵¹, was a gift from Prof Kenji Watanabe, University of Shizuoka, and the vectors pYFAC-riboB, pYFAC-pyroA, pYFAC-CH2, pYFAC-CH3, pYFAC-CH4 were built previously¹⁵. In all cases when amplifying *P_{gpdA}* and *T_{trpC}* consisted in the sequences delimited in the expression cassette from pBARGPE1²⁹, (obtained from the Fungal Genetics Stock Centre) or the modified version pBARGPE1-LIC⁵². To clone dSpCas9-VPR it was amplified from pAG414GPD-dCas9-VPR¹⁸, which was a gift

from George Church (Addgene plasmid #63801). dLbCas12a^{D832A} was amplified from a plasmid kindly provided by Christian Pflüger which was constructed from pY027⁵³, a gift from Feng Zhang (Addgene plasmid # 84742), by site-directed mutagenesis. and fused to VPR amplified from pAG414GPD-dCas9-VPR¹⁸. *P_{elcA}* was amplified from pYFAC-CH6¹⁵. The coding sequence of *mCherry* was amplified from pMP7601⁵⁴ which was a gift from Alex Andrianopoulos (University of Melbourne). *A. nidulans* sequences were PCR amplified from *A. nidulans* LO8030 gDNA (chromosomal coordinates indicated in Supplementary Table 5)⁵⁵. *AfP_{U3}* was amplified from *Aspergillus fumigatus* 293 gDNA. And adapted version of pGEM-T (Promega) was used to build the Step 1 crRNA and sgRNA cloning vector. The Cas9 sgRNA cloning cassette was synthesised as gBlock and re amplified when fused to *AfP_{U3}* (Sequence at Supplementary note 1). *P_{gpdA}* crRNA cloning cassette was created by annealed oligo cloning (Sequence at Supplementary note 1). Bsmbl domesticated one-step-cloning vector pCRI008 was built by PCR site directed mutagenesis of PYFAC-pyroA parts (Supplementary Fig. 4a).

sgRNA and crRNA design and cloning

The target sequences of each crRNA or sgRNA are listed in Supplementary Table 6, along with the PAM sequence and relative distance to target gene start codon and TSS⁵⁵. The spacers were also verified to pass the bioinformatic off-target test against *A. nidulans* FGSCA4 genome sequence with EuPaGDT⁵⁶. All crRNA and sgRNA were synthesised as oligonucleotides with overhangs, as listed in Supplementary Table 7. Oligos were mixed in equal proportion (10nM), annealed on a thermocycler, phosphorylated in the case of crRNA arrays and ligated with T4 DNA ligase in previously Bsmbl digested vectors.

For some Cas12a crRNA, one-step cloning was possible in the fungal crRNA expression vector pCRI008. For the rest, crRNA were cloned by a 2-vector cloning procedure (Supplementary Fig. 4c). In that case, oligos with encoded crRNA were first cloned into the pGEM-T derived vector pCRI007, and the expression cassette further PCR amplified with primers that reconstituted full *P_{gpdA}* and added homology arms. The amplicon was then cloned to the final YFAC fungal vector with homology-based cloning.

For Cas9 sgRNA, the sgRNAs were first cloned into pCRI010, and the PacI NotI flanked expression cassette digested, purified and ligated to a PacI NotI digested pCRI011 reporter vector.

A. nidulans strains construction and transformation

A. nidulans strains with either dCas9-VPR and dCas12a-VPR chromosomal expression cassettes were created by polyethylene glycol (PEG)-calcium-based transformation as in Lim et al.⁵⁷ with a previously linearised vector containing 1kb homology regions to facilitate

homologous recombination in *A. nidulans* 8030 *stcJΔ* locus. The fragment also contained the *Bar* marker, and colonies were selected for resistance to glufosinate extracted from Basta as in Li et al.¹⁶ and the event confirmed by diagnostic PCR. Complete genotype of the parental strains is listed in Supplementary Table 4.

For each transformant strain genotype of the protoplasts used and vectors transformed are listed in Supplementary Table 4, along with the strategy to supplement all auxotrophies. Protoplasts of *A. nidulans* LO8030, dCas-VPR expressing parental strains were prepared from germlings as in Lim et al.⁵⁷, mixed with a quarter volume PEG 60% to a final concentration of 10⁸ protoplasts per ml and frozen at -80 °C for later use. AMA1-vectors were transformed into *A. nidulans* protoplasts modifying Lim et al. 2012⁵⁷ in order to minimise the required transformation volume. In a 2 mL microcentrifuge tube, 60 µL of thawed protoplast solution was incubated with 50 µL of STC buffer and 3 µg of each plasmid contained in maximum total volume of 10 µL. After 20 mins of incubation on ice 350 µL of the calcium PEG 60% mix was added and mixed gently by inversion, followed by a 20 min incubation at room temperature. After adding 1 mL of STC buffer the mix was spread on solid glucose minimal media (GMM) stabilised with sorbitol (SMM), that were then incubated for three days at 37 °C to generate transformant colonies.

Fluorescence Microscopy

Spores from individual colonies were grown overnight in an incubator when 37° C , unless other incubation temperature specified, in small petri dishes containing liquid GMM to obtain mycelia. Samples grown at 30 °C were incubated overnight, while samples at 25 °C were grown for two days in order to harvest comparable mycelial growth. Fluorescence images were captured on the epifluorescence inverted microscope Eclipse Ti2 (Nikon), using Plan Apo λ 10x /0.45 numerical aperture (NA) objective lens (Nikon) and a Camera DS-Qi2 (Nikon) controlled by NIS Elements Advanced Research (Nikon). Fluorescent microscopy was carried out under a mCherry filter set (562/40 nm excitation, 593 nm dichroic beamsplitter, and 641/75 nm emission), using an 800 ms exposure and 9.6x analog gain unless specified otherwise. Brightfield images captured at a 300 ms exposure time with 1x analog gain. Images were recorded using NIS-Elements Advanced Research software package (Nikon).

Culture conditions and crude extract preparation

For each strain, three separate transformant colonies were picked as replicates for culture analysis and re-streaked individually in a solidified GMM plate to be cultivated for three days at 37 °C to produce spores. Spores were harvested from plates in 0.1% Tween 80 and counted under Neubauer chamber, 2x10⁸ spores were inoculated into 250-ml flasks containing 50 ml

liquid GMM medium as described previously¹⁵, additionally adding ampicillin to 50 µg mL⁻¹ and supplementing with riboflavin, uracil uridine, pyridoxine as indicated in Supplementary Table 4. Cultures were grown for 2.5 days with shaking set at 200 rpm and 37 °C, unless other temperature indicated. In the case only of the samples needing *P_{alcA}* promoter induction, cyclopentanone at a final concentration of 10 mM was added to the medium after 18 h of incubation. At the end of the culture, 20 mL of media was collected in 50-mL Falcon tubes by filtration with Miracloth. The metabolites were extracted from the liquid culture with 20 mL of an organic solvent mixture containing ethyl acetate, methanol and acetic acid (89.5:10:0.5 ratio). The crude extracts were dried down *in vacuo* and re-dissolved in 0.3 mL of methanol for LC-DAD-MS analysis.

Metabolic profile analysis by LC-DAD-MS

The analyses of the metabolite profiles were performed on an Agilent 1260 liquid chromatography (LC) system coupled to a diode array detector (DAD) and an Agilent 6130 Quadrupole mass spectrometer (MS) with an electrospray ionisation (ESI) source. In all cases 3 µL of the methanol dissolved crude extract was injected. Chromatographic separation was performed at 40 °C using a Kinetex C18 column (2.6 µm, 2.1 mm i.d. 3 100 mm; Phenomenex). Chromatographic separation was achieved with a linear gradient of 5-95% acetonitrile-water (containing 0.1% v/v formic acid) in 10 minutes followed by 95% acetonitrile for 3 minutes, with a flow rate of 0.70 mL min⁻¹. For the multiple target CRISPRa experiments, the gradient was extended to 20 min for better separation. The MS data were collected in the m/z range 100–1000 in positive ion mode and UV observed at DAD λ=254.0±4.0 nm.

Peak areas were determined by peak integration of DAD λ=254 nm chromatogram using Masshunter Workstation Qualitative Analysis (Agilent). To quantify microperfuraneone (**1**) samples were compared to a calibration curve. To this end, a standard of **1** was prepared by weighing approximately 14 mg of purified **1** and diluting in methanol. This procedure was repeated independently 3 times (Supplementary Fig. 18a), and a representative regression fit to zero was used to quantify **1** (Supplementary Fig. 18b). The coefficient was used to extrapolate the concentrations in the crude extract to the culture media concentrations.

For the calculated additive of single crRNA mediated production of **1** in Fig. 2e, the negative control mean was added to the summation of the difference between the mean of each individual crRNA production and the negative control mean, for the four crRNAs tested.

LC-MS/MS analysis

Selected samples were analysed by LC-MS/MS on a Thermo Scientific Fusion Orbitrap coupled to a Thermo Ultimate 3000 UHPLC. The column used was an Agilent Poroshell 120

SB-C18 (2.1 x 30 mm, 2.7 μ m) with a 20 min linear gradient of 5 – 95% acetonitrile-water containing 0.1% v/v formic acid. Precursor ion data was collected for m/z 200 to 300 Da in positive ion mode. Fragmentation was achieved with the higher-energy collisional dissociation cell set to a collision energy of 15. Fragment identification was aided by CFM-ID³⁷ predictions based on hypothesized structures.

Compound isolation and NMR structural characterization

For the microperfuranone (**1**) standard purification, 2 L of 2-days culture media from strain 52 (Supplementary Table 4), after induction, was extracted with a mix of ethyl acetate, methanol and acetic acid (89.5:10:0.5). The crude extract was dried *in vacuo*, resuspended in methanol and loaded onto a Sephadex LH-20 (GE Healthcare) column for fractionation. Fractions containing the target compound were combined and further purified by semi-prep HPLC with a C18 column (Grace, 5 μ m, 10 x 250 mm) (isocratic, 40% acetonitrile-water, 4.3mL min⁻¹).

For purification of dehydromicroperfuranone (**2**) peaks 4 L of 2-days culture media from strain 54 (Supplementary Table 4), after induction, was loaded onto a customized Diaion HP-20 (Sigma) column pre-equilibrated with water. The column was then flushed with 2 column-volume of water and eluted with methanol. The eluent was dried *in vacuo*. The crude extract was resuspended with methanol and fractionated using the Sephadex LH-20 column. Fractions containing the target peaks were combined and further purified by Semiprep HPLC with a C18 Preparative Cartridge (Agilent, 5 μ m, 21.2 x 150 mm). A gradient method (55% acetonitrile-water to 85% acetonitrile-water in 12 mins, 10 mL min⁻¹) was applied for the separation of peak III with peaks I-III.

For structural characterisation of **1** and **2**, nuclear magnetic resonance (NMR) spectra were collected on Bruker Avance IIIHD 500/600MHz NMR spectrometers, with either CDCl₃-*d* or MeOD-*d*₄ as solvents. NMR data in CDCl₃ was in good agreement with the published data (Supplementary Table 2; Supplementary Table 3)

Computational analysis of *A. nidulans* features

The genome assembly and corresponding gene annotations for *A. nidulans* FGSC A4 were obtained from FungiDB (denoted version 46)³³ Coordinates of predicted BGCs were obtained from the *A. nidulans* portal on the Joint Genome Institute's MycoCosm resource⁵⁸. The genome was parsed for gene features using Python scripts. Genes falling within cluster boundaries were grouped, forming an additional dataset to facilitate comparison between the whole genome and BGC genes.

Lengths of 5' UTRs were determined for all genes and BGC genes, based on features when available, filtering the genes with 5' UTRs equal zero. Histograms for each dataset were plotted using the Matplotlib library.

To determine the frequency of Cas9 and Cas12a PAM sites, upstream regions for all genes were isolated by taking up to 400 bp upstream of the start codon. When intergenic distance was less than 400 bp, the distance between the start codon and the end of the previous gene was used. Frequencies of the different PAM sites were obtained through regular expression searches of the PAM sequences considering both strands. Histograms for each dataset were plotted as mentioned above.

Statistical analysis

Statistical analysis was done using GraphPad Prism 8.3.0. All data were analysed with three biological replicates and Two-sided Welch's T-test with Holm-Šídák multiplicity correction per figure, using an alpha of 0.05. All Welch's T-test P-values calculated for each experiment along the details for the multiplicity adjustment are found in Supplementary Table 9.

Acknowledgements

Y.H.C. and this project is supported by an ARC Future Fellowship (FT160100233). I.R. is recipient of an UWA PhD Scholarship, J.H. and C.L.M.G. on Australian Government Research Training Program Scholarships. NMR and LC-MS/MS were performed at the UWA Centre for Microscopy, Characterisation and Analysis (CMCA). We thank Berl Oakley for *A. nidulans* LO8030 strain, and Christian Pflüger and Andrew Piggott for helpful discussion.

Data Availability

All relevant data generated during this study are available from the corresponding author on reasonable request. Main plasmids will be made available in Addgene, other plasmids are available under request.

Code Availability

All Python code used in these analyses is implemented in a Jupyter notebook which is available at https://github.com/gamcil/5_UTR_analysis/ alongside accompanying data.

Competing interests

The authors declare no competing interests.

Author contributions

I.R and Y.H.C conceived the project. I.R., C.W. and Y.H.C. wrote the manuscript. I.R. designed the constructs. I.R., C.W. and R.W. contributed to cloning. I.R. and C.W. performed the experiments and the data analysis. J.H. performed the NMR structural elucidation. C.L.M.G. wrote the code for computational analysis.

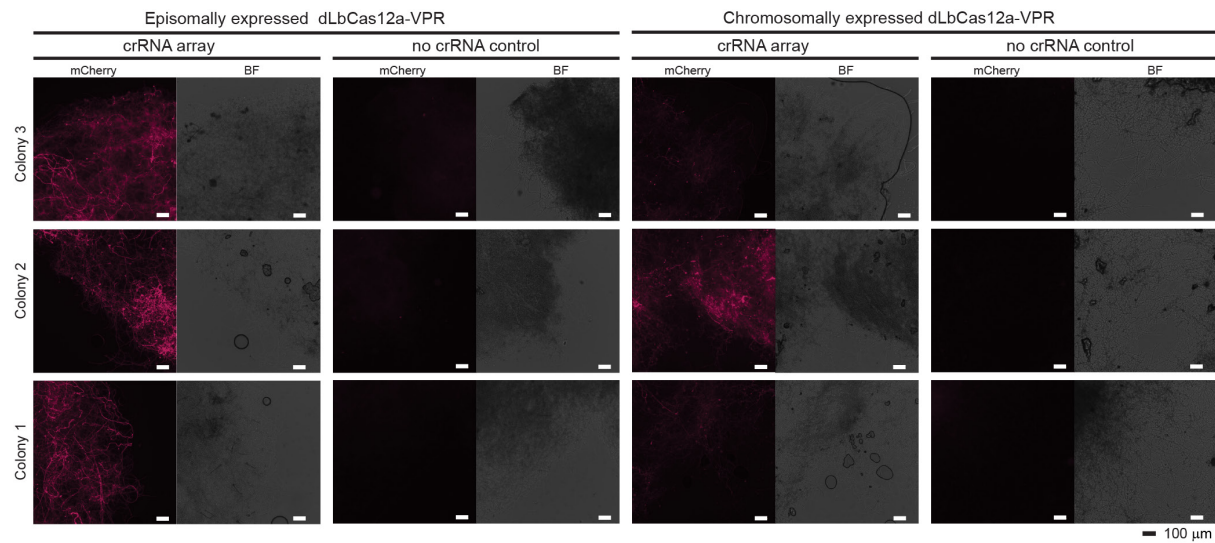
References

- Keller, N. P. Fungal secondary metabolism: regulation, function and drug discovery. *Nature Reviews Microbiology* **17**, 167–180 (2019).
- Rutledge, P. J. & Challis, G. L. Discovery of microbial natural products by activation of silent biosynthetic gene clusters. *Nature Reviews Microbiology* **13**, 509–523 (2015).
- Rokas, A., Wisecaver, J. H. & Lind, A. L. The birth, evolution and death of metabolic gene clusters in fungi. *Nature Reviews Microbiology* **16**, 731–744 (2018).
- Pfannenstiel, B. T. & Keller, N. P. On top of biosynthetic gene clusters: How epigenetic machinery influences secondary metabolism in fungi. *Biotechnology Advances* **37**, 1–14 (2019).
- Alberti, F., Foster, G. D. & Bailey, A. M. Natural products from filamentous fungi and production by heterologous expression. *Appl. Microbiol. Biotechnol.* **101**, 493–500 (2017).
- Kjærboelling, I., Mortensen, U. H., Vesth, T. & Andersen, M. R. Strategies to establish the link between biosynthetic gene clusters and secondary metabolites. *Fungal Genetics and Biology* **130**, 107–121 (2019).
- Gilchrist, C. L. M., Li, H. & Chooi, Y. H. Panning for gold in mould: Can we increase the odds for fungal genome mining? *Org. Biomol. Chem.* **16**, 1620–1626 (2018).
- Yeh, H. H. *et al.* Resistance Gene-Guided Genome Mining: Serial Promoter Exchanges in *Aspergillus nidulans* Reveal the Biosynthetic Pathway for Fellutamide B, a Proteasome Inhibitor. *ACS Chem. Biol.* **11**, 2275–2284 (2016).
- Bergmann, S. *et al.* Genomics-driven discovery of PKS-NRPS hybrid metabolites from *Aspergillus nidulans*. *Nat. Chem. Biol.* **3**, 213–217 (2007).
- Grau, M. F. *et al.* Hybrid Transcription Factor Engineering Activates the Silent Secondary Metabolite Gene Cluster for (+)-Asperlin in *Aspergillus nidulans*. *ACS Chem. Biol.* **13**, 3193–3205 (2018).
- He, Y. *et al.* Recent advances in reconstructing microbial secondary metabolites biosynthesis in *Aspergillus* spp. *Biotechnol. Adv.* **36**, 739–783 (2018).
- Clevenger, K. D. *et al.* A scalable platform to identify fungal secondary metabolites and their gene clusters. *Nat. Chem. Biol.* **13**, 895–901 (2017).
- Chiang, Y. M. *et al.* An efficient system for heterologous expression of secondary metabolite genes in *Aspergillus nidulans*. *J. Am. Chem. Soc.* **135**, 7720–7731 (2013).
- Liu, L., Tang, M.-C. & Tang, Y. Fungal Highly Reducing Polyketide Synthases Biosynthesize Salicylaldehydes that are Precursors to Epoxycyclohexenol Natural Products. *J. Am. Chem. Soc.* **141**, 19538–19541 (2019).
- Hu, J. *et al.* Heterologous biosynthesis of elsinochrome A sheds light on the formation of the photosensitive perylenequinone system. *Chem. Sci.* **10**, 1457–1465 (2019).
- Li, H. *et al.* Genomics-Driven Discovery of Phytotoxic Cytochalasans Involved in the Virulence of the Wheat Pathogen *Parastagonospora nodorum*. *ACS Chem. Biol.* (2019). doi:10.1021/acscchembio.9b00791
- Dominguez, A. A., Lim, W. A. & Qi, L. S. Beyond editing: Repurposing CRISPR-Cas9 for precision genome regulation and interrogation. *Nat. Rev. Mol. Cell Biol.* **17**, 5–15 (2016).
- Chavez, A. *et al.* Highly efficient Cas9-mediated transcriptional programming. *Nat. Methods* **12**, 326–328 (2015).

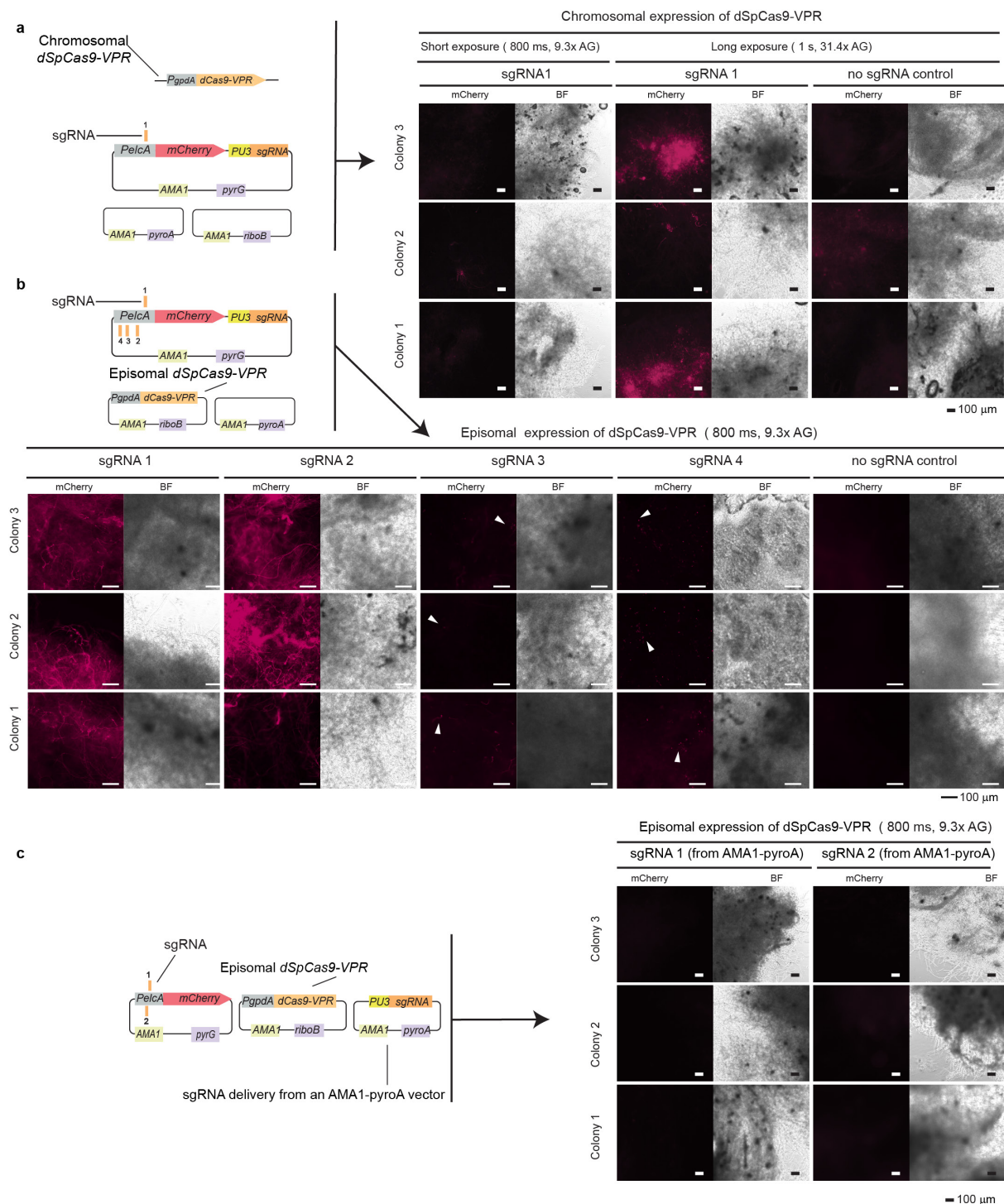
19. Tak, Y. E. *et al.* Inducible and multiplex gene regulation using CRISPR-Cpf1-based transcription factors. *Nat. Methods* **14**, 1163–1166 (2017).
20. Zalatan, J. G. *et al.* Engineering complex synthetic transcriptional programs with CRISPR RNA scaffolds. *Cell* **160**, 339–350 (2015).
21. Peng, R. *et al.* CRISPR/dCas9-mediated transcriptional improvement of the biosynthetic gene cluster for the epothilone production in *Myxococcus xanthus*. *Microb. Cell Fact.* **17**, 1–12 (2018).
22. Deaner, M. & Alper, H. S. Systematic testing of enzyme perturbation sensitivities via graded dCas9 modulation in *Saccharomyces cerevisiae*. *Metab. Eng.* **40**, 14–22 (2017).
23. Schwartz, C., Curtis, N., Löbs, A. K. & Wheeldon, I. Multiplexed CRISPR Activation of Cryptic Sugar Metabolism Enables *Yarrowia Lipolytica* Growth on Cellobiose. *Biotechnol. J.* **13**, 1–7 (2018).
24. Aleksenko, A. & Clutterbuck, A. J. Autonomous plasmid replication in *Aspergillus nidulans* AMA1 and MATE elements. *Fungal Genet. Biol.* **21**, 373–387 (1997).
25. Chiang, Y. M. *et al.* Development of Genetic Dereplication Strains in *Aspergillus nidulans* Results in the Discovery of Aspercryptin. *Angew. Chemie - Int. Ed.* **55**, 1662–1665 (2016).
26. Chooi, Y. H. *et al.* Functional genomics-guided discovery of a light-activated phytotoxin in the wheat pathogen *Parastagonospora nodorum* via pathway activation. *Environ. Microbiol.* **19**, 1975–1986 (2017).
27. Fonfara, I., Richter, H., Bratovič, M., Le Rhun, A. & Charpentier, E. The CRISPR-associated DNA-cleaving enzyme Cpf1 also processes precursor CRISPR RNA. *Nature* **532**, 517–521 (2016).
28. Zhong, G., Wang, H., Li, Y., Tran, M. H. & Farzan, M. Cpf1 proteins excise CRISPR RNAs from mRNA transcripts in mammalian cells. *Nat. Chem. Biol.* **13**, 839–841 (2017).
29. Pall, M. L. & Brunelli, J. P. A series of six compact fungal transformation vectors containing polylinkers with multiple unique restriction sites. *Fungal Genet. Rep.* **40**, 59–62 (1993).
30. Nødvig, C. S. *et al.* Efficient oligo nucleotide mediated CRISPR-Cas9 gene editing in *Aspergilli*. *Fungal Genet. Biol.* **115**, 78–89 (2018).
31. Yeh, H. H. *et al.* Molecular genetic analysis reveals that a nonribosomal peptide synthetase-like (NRPS-like) gene in *Aspergillus nidulans* is responsible for microperforanone biosynthesis. *Appl. Microbiol. Biotechnol.* **96**, 739–748 (2012).
32. Sibthorp, C. *et al.* Transcriptome analysis of the filamentous fungus *Aspergillus nidulans* directed to the global identification of promoters. *BMC Genomics* **14**, 847 (2013).
33. Basenko, E. Y. *et al.* FungiDB: An integrated bioinformatic resource for fungi and oomycetes. *J. Fungi* **4**, (2018).
34. Jensen, M. K. Design principles for nuclease-deficient CRISPR-based transcriptional regulators. *FEMS Yeast Res.* **18**, 1–11 (2018).
35. Andersen, M. R. *et al.* Accurate prediction of secondary metabolite gene clusters in filamentous fungi. *Proc. Natl. Acad. Sci.* **110**, E99–E107 (2012).
36. Hamasaki, T., Nakajima, H., Yokota, T. & Kimura, Y. A New Metabolite, 3-Carboxy-2,4-diphenyl-but-2-enoic Anhydride, Produced by *Aspergillus nidulans*. *Agric. Biol. Chem.* **47**, 891–892 (1983).
37. Allen, F., Pon, A., Wilson, M., Greiner, R. & Wishart, D. CFM-ID: A web server for annotation, spectrum prediction and metabolite identification from tandem mass spectra. *Nucleic Acids Res.* **42**, (2014).
38. Oakley, C. E. *et al.* Discovery of McrA, a master regulator of *Aspergillus* secondary metabolism. *Mol. Microbiol.* **103**, 347–365 (2017).
39. Moreno-Mateos, M. A. *et al.* CRISPR-Cpf1 mediates efficient homology-directed repair and temperature-controlled genome editing. *Nat. Commun.* **8**, 2024 (2017).
40. Dix, N. J., Webster, J., Dix, N. J. & Webster, J. Fungi of Extreme Environments. in

- 655 *Fungal Ecology* 322–340 (1995). doi:10.1007/978-94-011-0693-1_12
- 656 41. Kleinstiver, B. P. *et al.* Engineered CRISPR–Cas12a variants with increased activities
657 and improved targeting ranges for gene, epigenetic and base editing. *Nat. Biotechnol.*
658 **37**, 276–282 (2019).
- 659 42. Yamano, T. *et al.* Crystal Structure of Cpf1 in Complex with Guide RNA and Target
660 DNA. *Cell* **165**, 949–962 (2016).
- 661 43. Yamano, T. *et al.* Structural Basis for the Canonical and Non-canonical PAM
662 Recognition by CRISPR–Cpf1. *Mol. Cell* **67**, 633–645.e3 (2017).
- 663 44. Zetsche, B. *et al.* Cpf1 Is a Single RNA-Guided Endonuclease of a Class 2 CRISPR-
664 Cas System. *Cell* **163**, 759–771 (2015).
- 665 45. Joung, J. K., Kleinstiver, B. & Sousa, A. Variants of CPF1 (CAS12a) With Altered
666 PAM Specificity. US patent 20190010481A1 (2019).
- 667 46. Sanson, K. R. *et al.* Optimized libraries for CRISPR–Cas9 genetic screens with
668 multiple modalities. *Nat. Commun.* **9**, 5416 (2018).
- 669 47. Campa, C. C., Weisbach, N. R., Santinha, A. J., Incarnato, D. & Platt, R. J.
670 Multiplexed genome engineering by Cas12a and CRISPR arrays encoded on single
671 transcripts. *Nat. Methods* **16**, 887–893 (2019).
- 672 48. Nihongaki, Y., Otabe, T., Ueda, Y. & Sato, M. A split CRISPR–Cpf1 platform for
673 inducible genome editing and gene activation. *Nat. Chem. Biol.* **15**, 882–888 (2019).
- 674 49. Howe, F. S. *et al.* CRISPRi is not strand-specific at all loci and redefines the
675 transcriptional landscape. *Elife* **6**, e29878 (2017).
- 676 50. Schindele, P. & Puchta, H. Engineering CRISPR/LbCas12a for highly efficient,
677 temperature-tolerant plant gene editing. *Plant Biotechnology Journal* (2019).
678 doi:10.1111/pbi.13275
- 679 51. Tsunematsu, Y. *et al.* Distinct mechanisms for spiro-carbon formation reveal
680 biosynthetic pathway crosstalk. *Nat. Chem. Biol.* **9**, 818–825 (2013).
- 681 52. Chooi, Y. H. *et al.* Genome mining of a prenylated and immunosuppressive polyketide
682 from pathogenic fungi. *Org. Lett.* **15**, 780–783 (2013).
- 683 53. Zetsche, B. *et al.* Multiplex gene editing by CRISPR–Cpf1 using a single crRNA array.
684 *Nat. Biotechnol.* **35**, 31–34 (2017).
- 685 54. Boyce, K. J., Bugeja, H. E., Weerasinghe, H., Payne, M. J. & Schreider, L. Strategies
686 for the molecular genetic manipulation and visualization of the human fungal
687 pathogen *Penicillium marneffei*. *Fungal Genet. Rep.* **59**, 1–12 (2012).
- 688 55. Cerqueira, G. C. *et al.* The *Aspergillus* Genome Database: Multispecies curation and
689 incorporation of RNA-Seq data to improve structural gene annotations. *Nucleic Acids*
690 *Res.* **42**, 705–710 (2014).
- 691 56. Tarleton, R. & Peng, D. EuPaGDT: a web tool tailored to design CRISPR guide RNAs
692 for eukaryotic pathogens. *Microb. Genomics* **1**, 1–7 (2015).
- 693 57. Lim, F. Y., Sanchez, J. F., Wang, C. C. C. & Keller, N. P. Toward awakening cryptic
694 secondary metabolite gene clusters in filamentous fungi. *Methods Enzymol.* **517**,
695 303–324 (2012).
- 696 58. Grigoriev, I. V. *et al.* MycoCosm portal: Gearing up for 1000 fungal genomes. *Nucleic*
697 *Acids Res.* **42**, (2014).

Supplementary Information

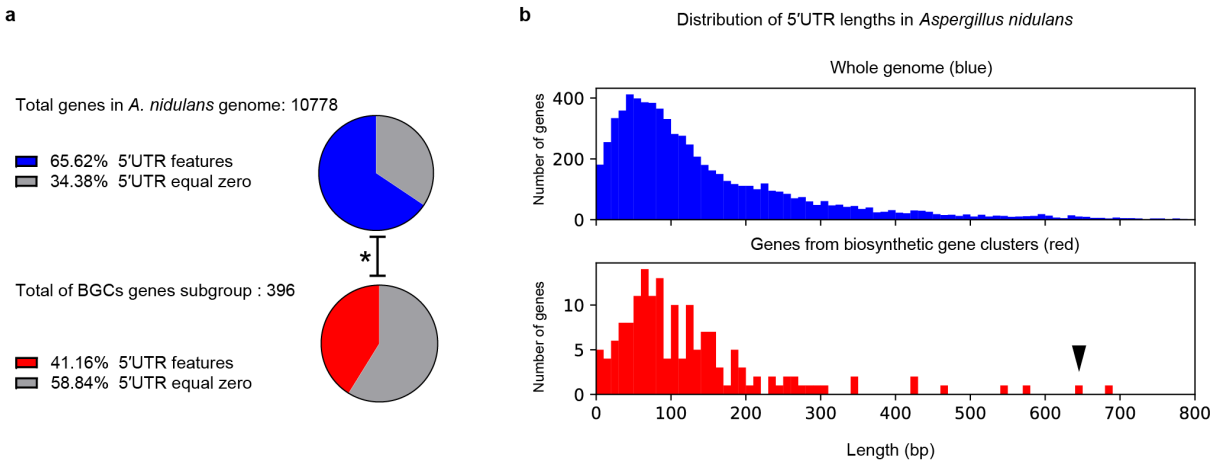


Supplementary Fig. 1: Activation of the fluorescent reporter P_{elcA} -mCherry by CRISPR/dLbCas12a-VPR. Fluorescence microscopy images of *A. nidulans* mycelia demonstrate mCherry fluorescence when the poly-crRNA array is present in both episomally and chromosomally expressed dLbCas12a-VPR systems, distinct from the no crRNA control. The spores for each sample were collected from three individual colonies and grown overnight in liquid stationary culture at 37 °C. Samples with similar mycelial growth were observed under mCherry filter and brightfield (BF). Scale bar 100 μm.

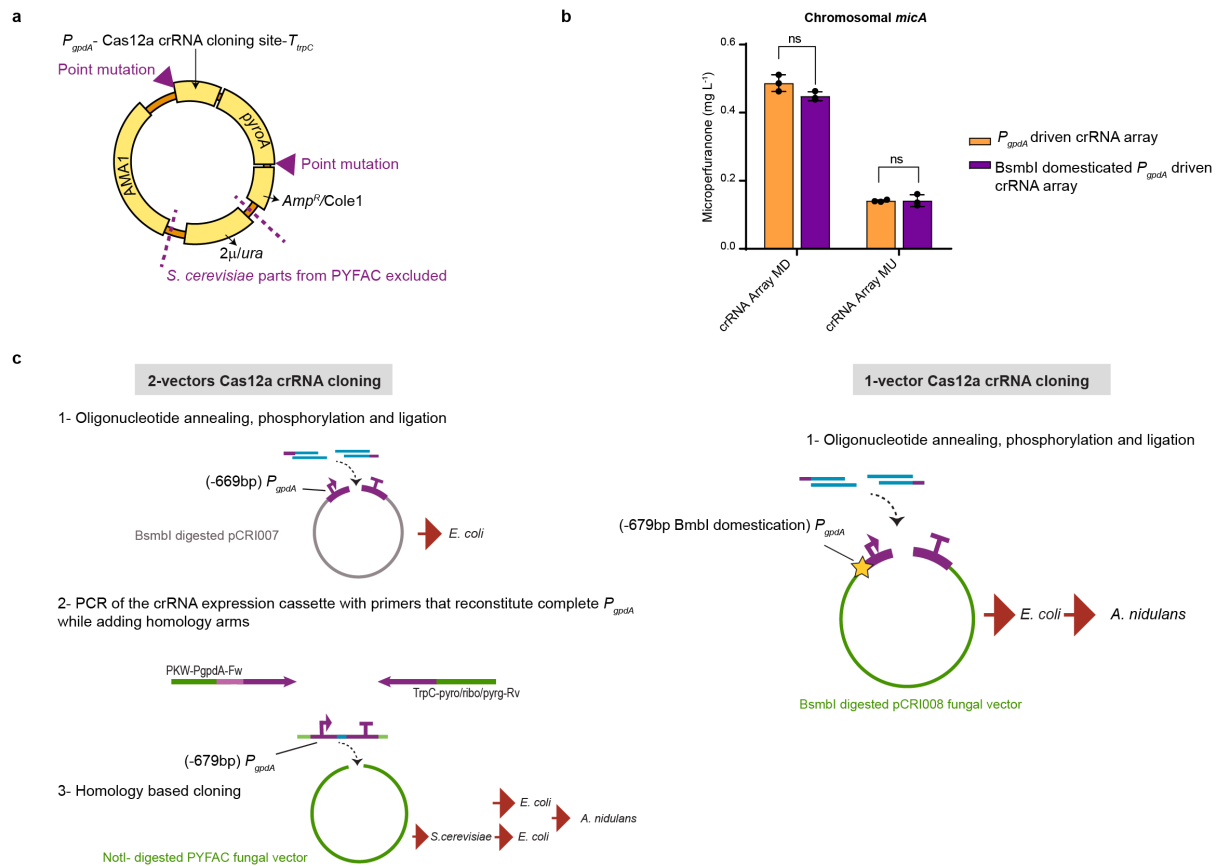


Supplementary Fig. 2. Activation of the fluorescent reporter *P_{elcA}-mCherry* by CRISPR/dSpCas9-VPR is dependent on CRISPRa components mode of delivery. **a.** CRISPRa samples with *dSpCas9-VPR* is chromosomally expressed and sgRNA 1 (presented in diagram) resulted in low activation the *mcherry* reporter, although samples were distinct to the no sgRNA control when observed at prolonged exposure times and increased sensitivity (1s exposure and 31.4x analog gain). **b.** *AMA1*-encoded CRISPR/dSpCas9-VPR system (presented diagrammatically) resulted in strong fluorescence observable in all mycelia at short exposure times when targeting the reporter construct with sgRNA 1 or sgRNA 2. The two

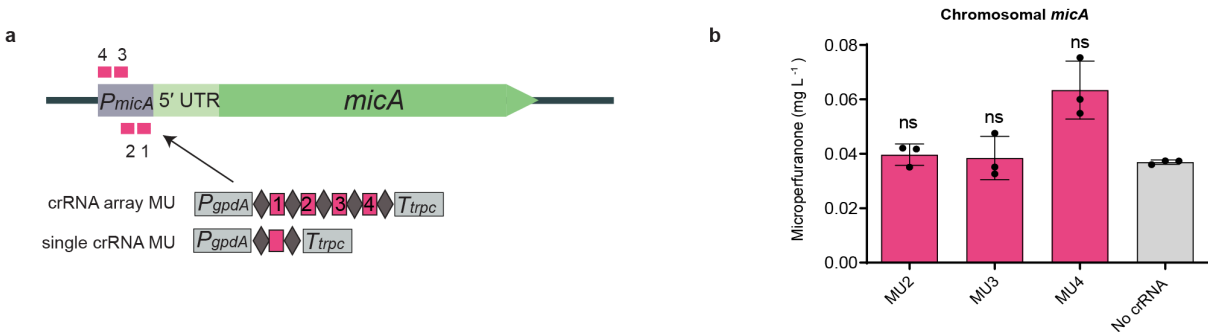
sgRNA targeting regions further away from the gene start codon (sgRNA 3 and sgRNA 4) resulted in low fluorescence localized in spores or isolated mycelia, but distinguishable from the no sgRNA negative control. Images are 2X digitally zoomed to show the fluorescence of the spores (white arrows). **c.** The strong activation by the episomally delivered dSpCas9-VPR system observed with sgRNA 1 and sgRNA 2 is abolished when the sgRNA is delivered encoded in a separate AMA1-pyro vector (represented in adjacent diagram). The spores for each sample were collected from three individual colonies and grown overnight in liquid stationary culture at 37 °C. Samples with similar mycelial growth were observed under mCherry filter and brightfield (BF). Scale bar 100 μm.



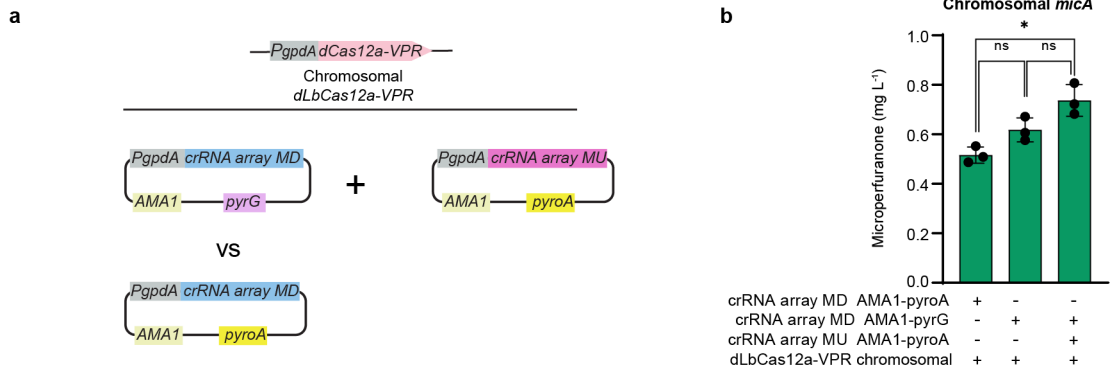
Supplementary Fig. 3. *Aspergillus nidulans* 5' UTR features **a.** Access to transcription starting site (TSS) information for CRISPRa targeting is limited in the current version of the *A. nidulans* genome. The proportion of genes that have annotated 5' UTR lengths greater than zero is smaller for BGCs compared to the whole genome. This could be due to the low expression of most BGCs genes in the growth conditions in which the transcriptomic data was acquired ¹. Asterisk represents the significant result of Fisher's exact test two-sided $p < 0.0001$. **b.** Distribution of 5' UTR length in *Aspergillus nidulans* genes for the whole genome (blue) and in genes that fall within BGC boundaries only (red), after filtering genes with no 5' UTR annotation. Arrow indicates the *micA* 5' UTR length.



Supplementary Fig. 4 . One-step cloning of Cas12a crRNA with pCRI008. A. Diagram of the Bsmbl domestication strategy used to create the vector pCRI008. Two point mutations were introduced, one in P_{gpdA} promoter from the crRNA expression cassette, and the other in the $pyroA$ marker terminator region. The components of pYFAC for replication in *Saccharomyces cerevisiae* were eliminated to avoid Bsmbl sites. **b.** No difference in microperfuraneone (1) activation mediated by CRISPRa is observed between systems with crRNA array expression driven by the original P_{gpdA} sequence (orange) and the Bsmbl domesticated version of P_{gpdA} (purple), confirming the null effect of the mutation. Titres of 1 (mg L⁻¹) values are the mean of three biological replicates, specific values of which are indicated as black dots, bars represent SD. Two-sided Welch's T-test was performed. Asterisk indicates P-value<0.05. Individual P-values are listed in Supplementary Table 9. **c.** The simplified one-vector cloning strategy with the Bsmbl-domesticated pCRI008 versus the original two-vector cloning strategy. In the two-vector strategy, a shorter P_{gpdA} lacking Bsmbl site was cloned into a pGEM-T backbone to create a vector (pCRI007) for type IIS restriction enzyme cloning. This crRNA cassette would be later be amplified by primers that would reconstitute the full P_{gpdA} sequence when incorporated into a fungal vector by homology-based cloning.

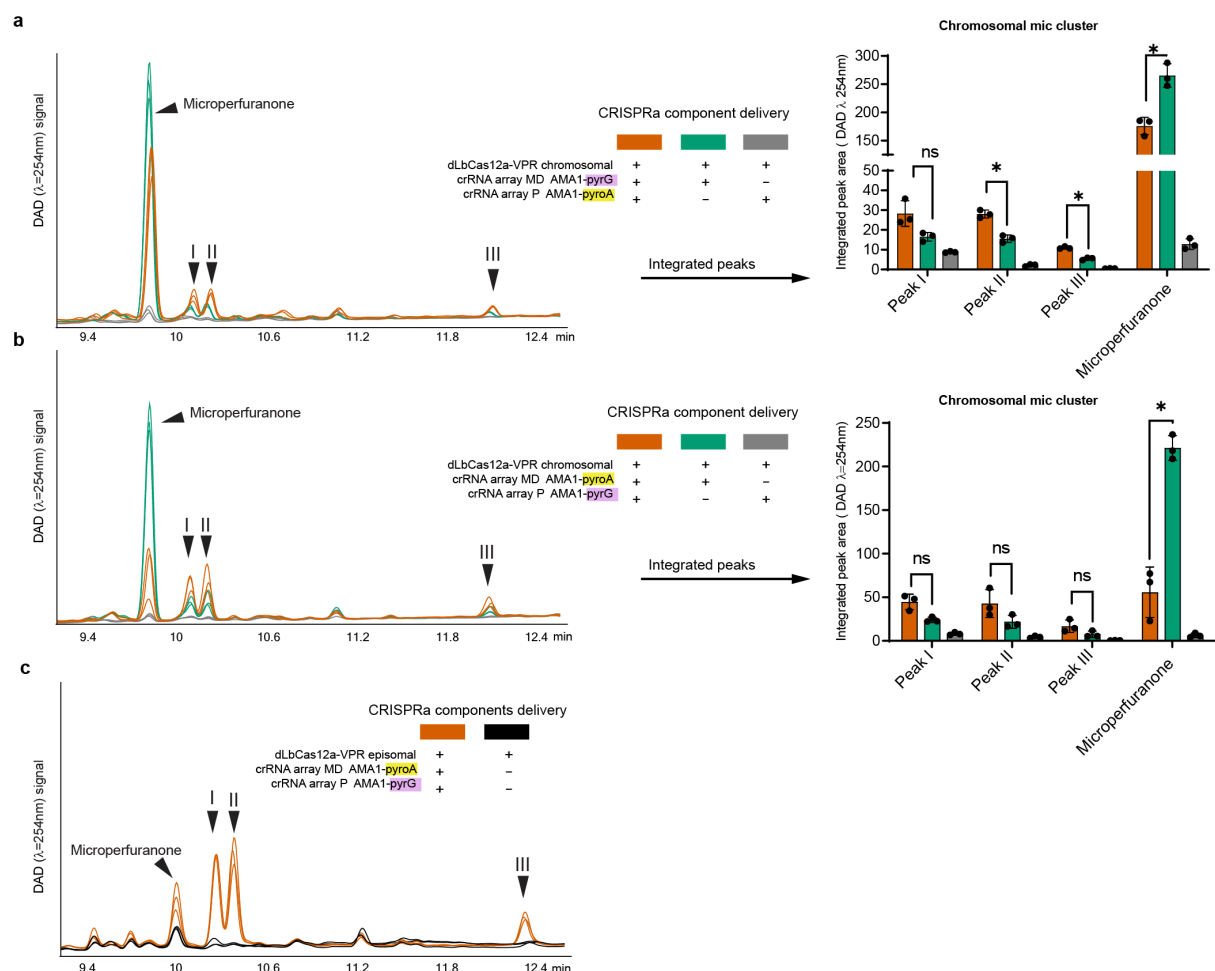


Supplementary Fig. 5. Individual MU crRNA tested do not result in significant activation. **a.** Chromosomal *micA* gene scheme with individual crRNA MU (magenta) target sites indicated. Numbers assigned to crRNA MD are indicative of targeting position in respect to *micA* TSS, with their position in the crRNA array MD also indicated in the scheme **b.** No significant changes in the production of microperfurane are observed targeting with single crRNAs compared to the no crRNA control. Microperfurane titre (mg L⁻¹) values are the mean of three biological replicates in which specific values are indicated as black dots, error bars represent SD. Two-sided Welch's T-test with Holm-Šídák multiplicity correction per figure was performed. Asterisk indicates corrected P-value<0.05. Individual P-values are listed in Supplementary Table 9.



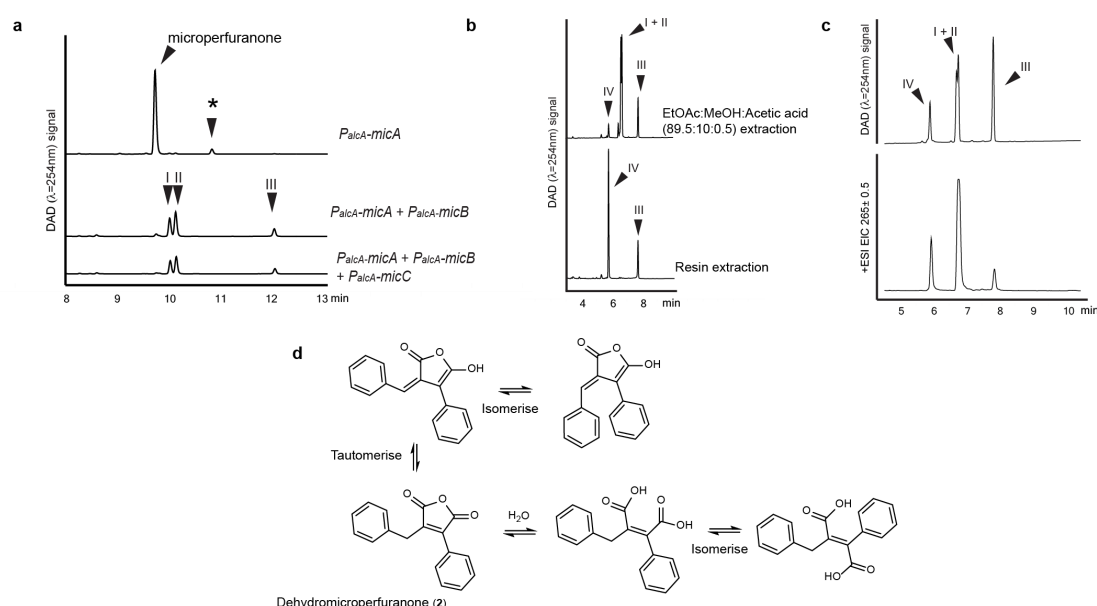
Supplementary Fig. 6. CRISPRa of *micA* with both MD and MU crRNA arrays. **a.** Overview of double crRNA array mediated activation of *micA* in strains harbouring chromosomally integrated *dLbCas12a-VPR*. In order to allow co-transformation of two crRNA arrays, crRNA array MD was re-cloned into an AMA1-pyrG vector. This allowed comparing the performance of crRNA array MD in both AMA1-pyrG and AMA1-pyroA vectors. **b.** Double crRNA array (8 crRNA) mediated activation of *micA* resulted in microperfurane titres higher than the four-crRNA array MD alone when delivered from AMA1-pyroA. However, there is no significant increase from the production observed by crRNA array MD alone when delivered from AMA1-pyrG. The differences in the production mediated by crRNA MD when using the markers *pyrG* and *pyroA* is not significant, suggests that the marker used for crRNA delivery might influence the system performance. Microperfurane titre (mg L⁻¹) values are the mean of three biological replicates, of which specific values are indicated as black dots, bars represent SD.

Two-sided Welch's T-test with Holm-Šídák multiplicity correction per figure was performed. Asterisk indicates corrected P-value<0.05, (ns) not significant. Individual P-values are listed in Supplementary Table 9.



Supplementary Fig. 7. Multiple gene activation of *mic* cluster. **a–b.** Overlaid DAD ($\lambda=254\text{ nm}$) chromatograms of acidified ethyl acetate mix media crude extracts from strains co-transformed with the multiple crRNA arrays MD and P (orange), crRNA array MD (green) and crRNA array P (grey) strains; combination in **a** for multiple targeting (orange), crRNA MD in AMA1-pyrG and crRNA P in AMA1-pyroA; combination in for **b** (orange), crRNA MD in AMA1-pyroA and crRNA P in AMA1-pyrG. Both multiple crRNA arrays (orange) for combinations **a** and **b** showed conversion of the precursor microperfurane to the peaks I–III. Compared to **a**, combination **b** showed a stronger decrease in the titre of the precursor microperfurane and higher titre of the peaks I–III. **c.** Expression of dLbCas12a-VPR from the multicopy AMA1-vector with the same crRNA array delivery combination as **b** resulted in a further increase of peaks I–III production relative to microperfurane. Chromatograms in **a,b,c** are represented at the same scale. Microperfurane titre (mg L^{-1}) values are the mean of three biological replicates, of which specific values are indicated as black dots, bars represent SD. Two-sided Welch's T-test with Holm-Šídák multiplicity correction per figure was performed. Asterisk

798 indicates corrected P-value<0.05, (ns) not significant. Individual P-values are listed in
799 Supplementary Table 9.

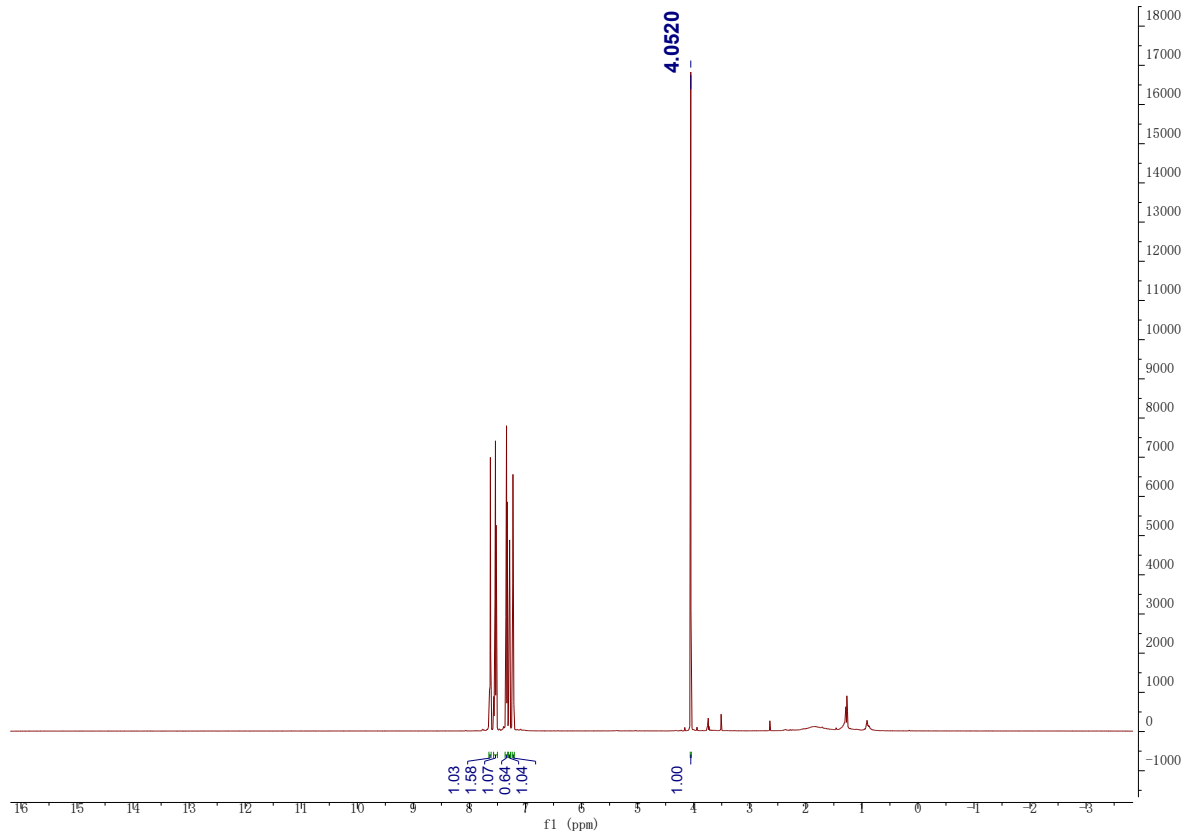


800

801 **Supplementary Fig. 8.** Verification of *mic* cluster product by promoter exchange and
802 dehydromicroperfurane isolation. **a.** DAD ($\lambda=254\text{ nm}$) chromatograms from *mic* cluster
803 genes (*micA*–*C*) expression from an alcohol inducible promoter (*P_{alcA}*). Overexpression of
804 *micA* results in the expected microperfurane peak and a smaller unidentified peak likely to
805 be a side product of microperfurane with *m/z* 251 (asterisk). Co-expression of *micA* and
806 *micB* resulted in the production of the peaks I–III peaks as expected. Co-expression of *micA*–
807 *C* results in the same metabolic profile of *micA*–*B*, indicating that *micC* is likely not necessary
808 to produce peaks I–III. All chromatograms run with a gradient of 20 min. **b.** Metabolic profile
809 of highly concentrated samples from culture media crude extract obtained when scaling up for
810 purification showing peaks I–III and a smaller IV of identical *m/z* 265 when extracted with
811 acidified ethyl acetate and methanol mix. When extracting the same media with a solid resin
812 we observe only the peaks IV and III. All chromatograms with a gradient of 10 min. **c.** LC-
813 DAD-MS analysis of the purified peak III used for NMR analysis (top, DAD chromatogram
814 $\lambda=254\text{ nm}$; bottom, extracted ion chromatogram *m/z* 265). The purified peak III NMR sample
815 in chloroform-*d*, which appeared as a pure single chemical entity based on ^1H and ^{13}C NMR
816 analysis (Supplementary Table 2, Supplementary Fig. 9 and 10), was dried and reconstituted
817 in methanol for the LC-DAD-MS analysis. LC-DAD-MS of co-purified peaks I–II shared the
818 same profile. ^1H NMR analysis of the reconstituted sample in methanol-*d* also showed that the
819 compounds existed as mixed forms (Supplementary Fig. 13 and 14). **d.** Possible
820 interconvertible forms of dehydromicroperfurane based on possible tautomerisation and *cis*-
821 *trans* isomerisation of maleic acid to fumaric acid. Note: *m/z* 283 was occasionally observed

822 to coexist with m/z 265 for the peaks I–IV suggesting that some of the m/z 265 ions detected
823 could be $[M+H-H_2O]^+$. However, it is difficult to determine which peaks is in which form as they
824 appear as a single peak in chloroform-*d* during NMR analysis and converted back to multiple
825 peaks during LC-DAD-MS.
826

827

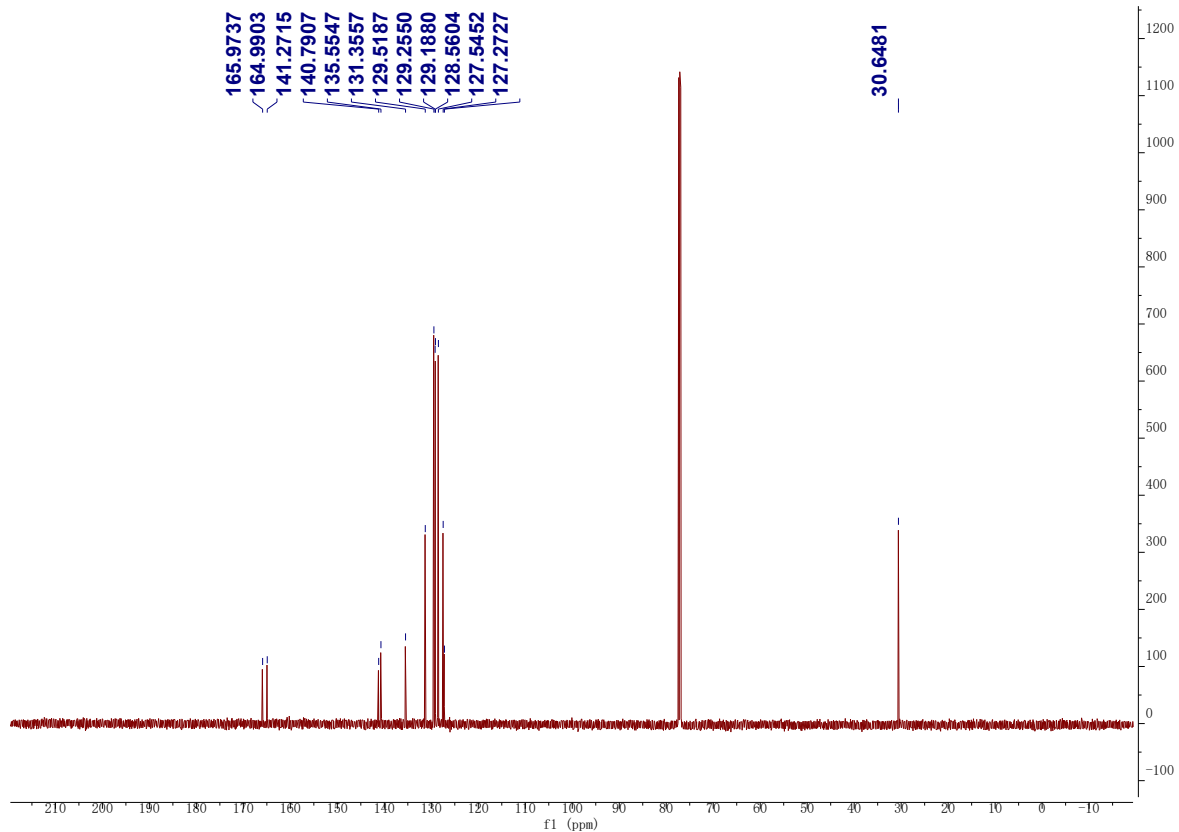


828

829

830

Supplementary Fig. 9 ^1H NMR spectrum (600 MHz) of purified peak III in CDCl_3-d .

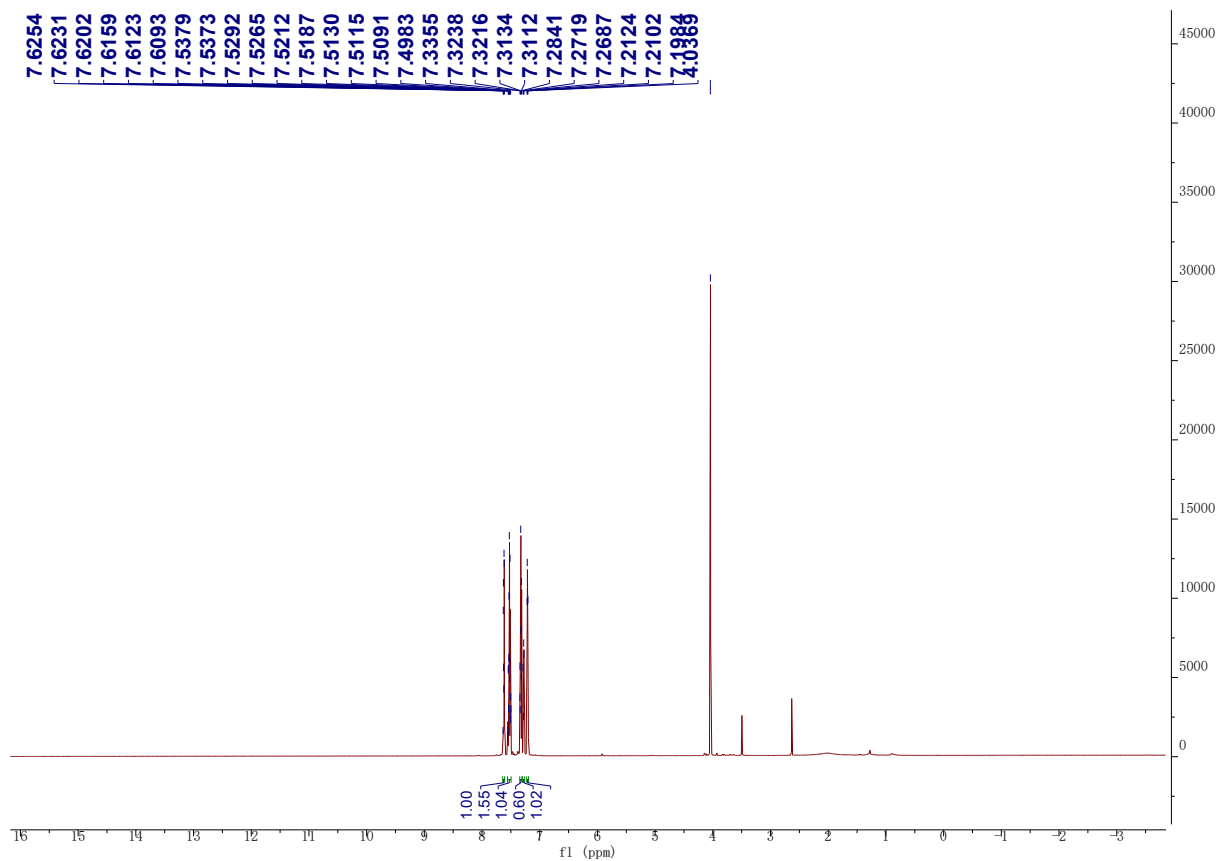


831

832

Supplementary Fig. 10 ^{13}C NMR spectrum (150 MHz) of purified peak III in CDCl_3-d .

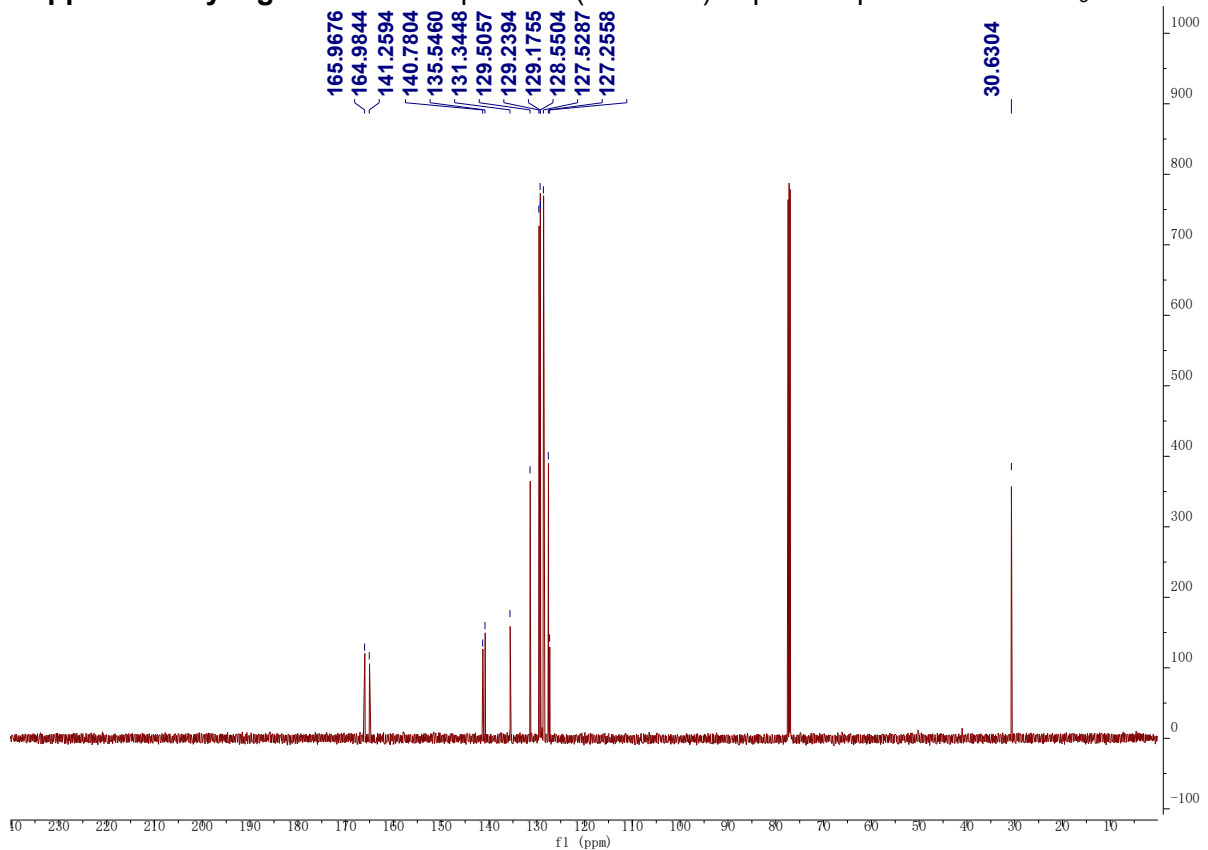
833



834

835

Supplementary Fig. 11 ¹H NMR spectrum (600 MHz) of purified peaks I-II in CDCl₃-d.

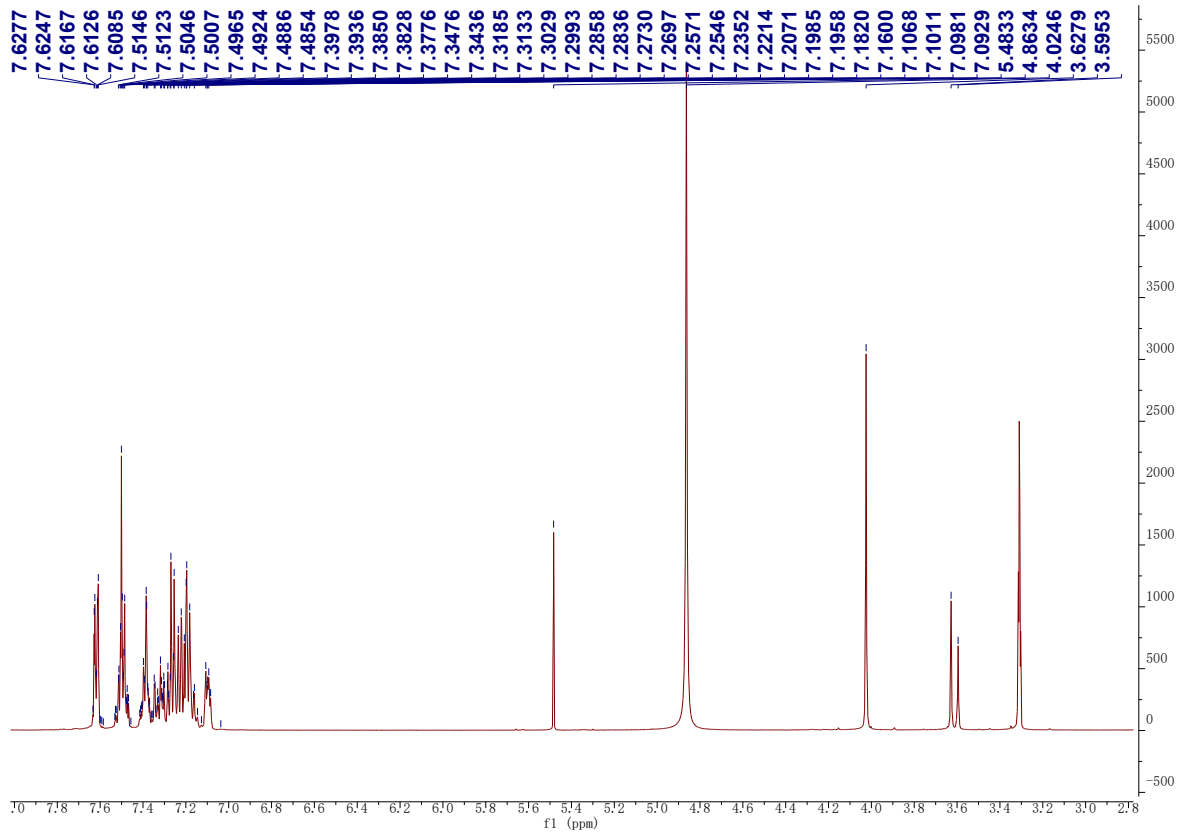


836

837

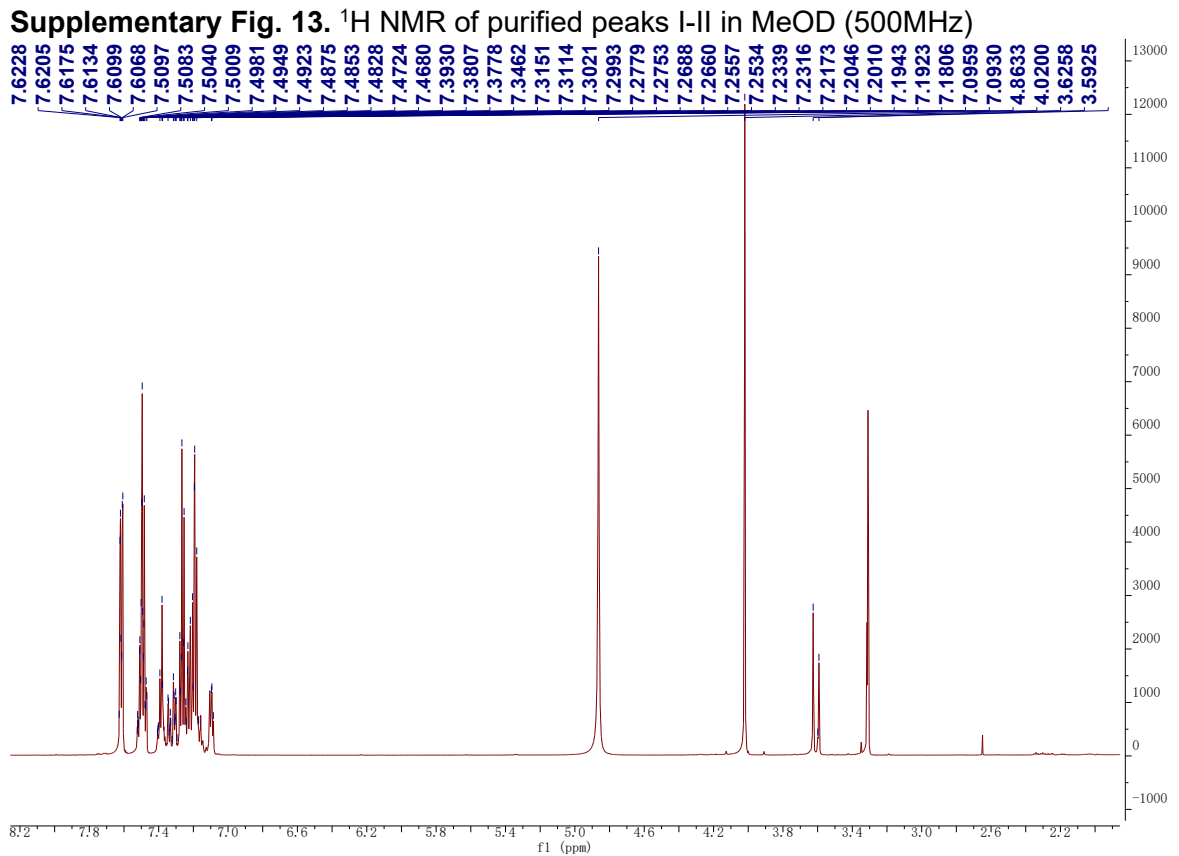
Supplementary Fig. 12 ¹³C NMR spectrum (150 MHz) of purified peaks I-II in CDCl₃-d.

838



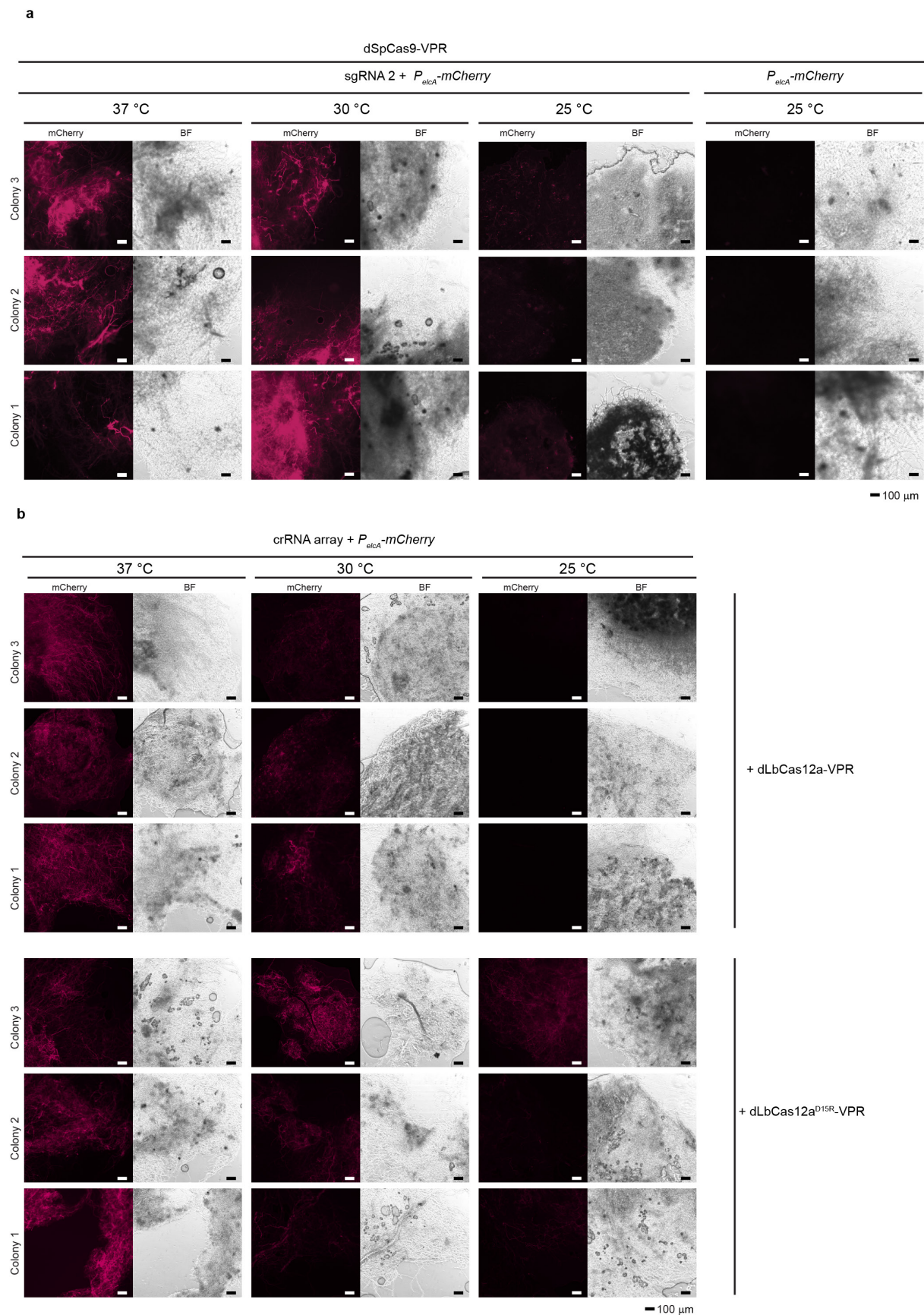
839

840



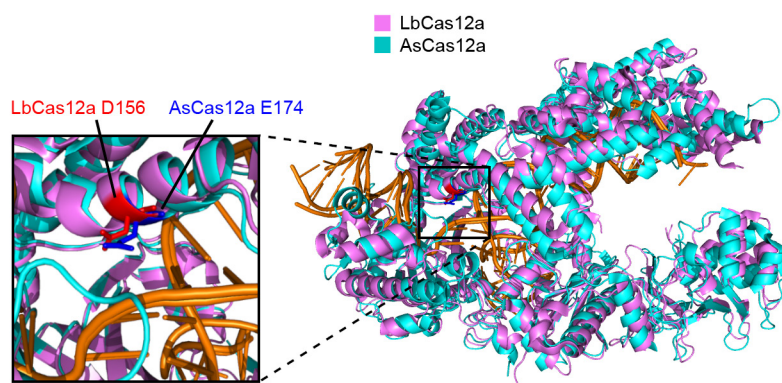
841

842

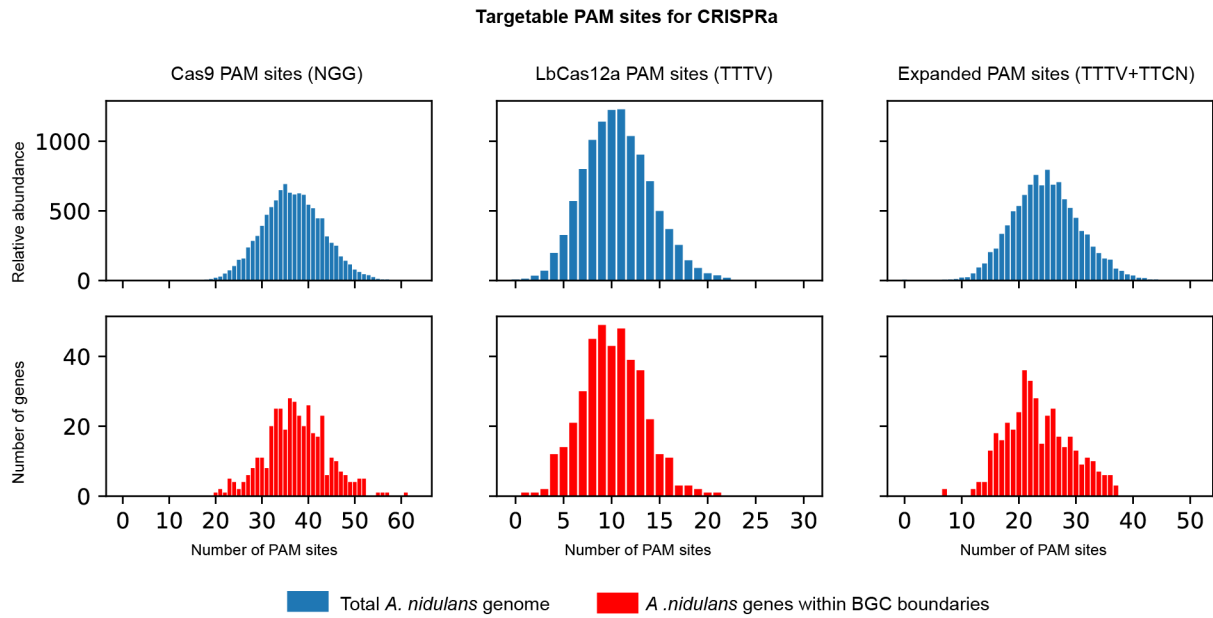


Supplementary Fig. 15 CRISPR-mediated activation of P_{elcA} -mcherry fluorescent reporter is limited at low temperatures . **a**. The activation observed in mycelia by CRISPR/dspCas9-VPR

at 37 °C is similar to that observed at 30 °C but lower at 25 °C in mycelia at a stage of equivalent growth to that observed in the other temperature conditions. Fluorescence at 25 °C was still distinguishable from the no sgRNA control. **b.** CRISPR/dLbCas12a-mediated activation was observed for mycelia grown at 37 °C and 30 °C but not observed at 25 °C. The variant dLbCas12a^{D156R}-VPR presents observable fluorescence signal at 25 °C unlike the original system. In all cases, the spores for each sample were collected from three individual colonies and grown in liquid stationary culture overnight in the case of 37 °C, and 30 °C and two days for the samples at 25°C. The photos represent the mCherry channel and bright-field (BF). Scale bar 100 µm.

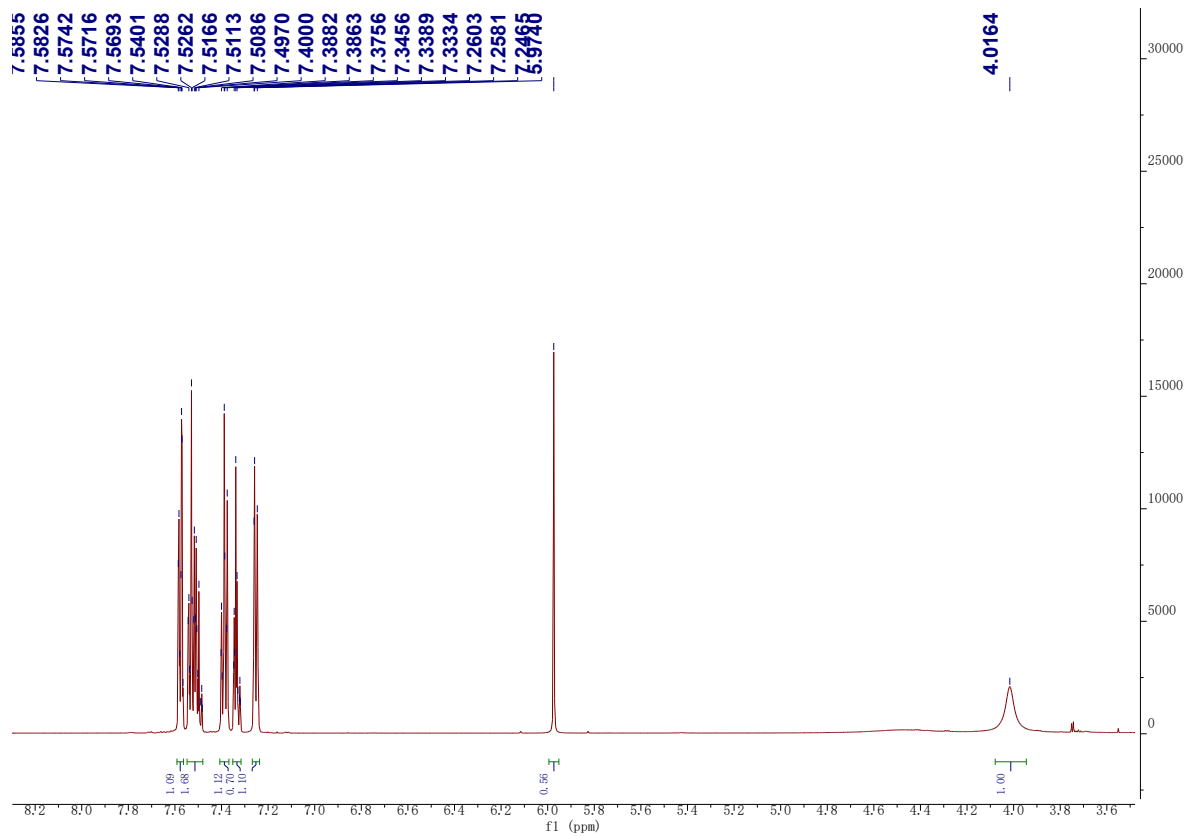


Supplementary Fig. 16 Protein alignment visualised in Pymol of LbCas12a (pink) and AsCas12a (light blue) crystal structures^{2,3} indicates that residue D156 from LbCas12a (Red) is an equivalent residue to E174 from AsCas12a (blue).



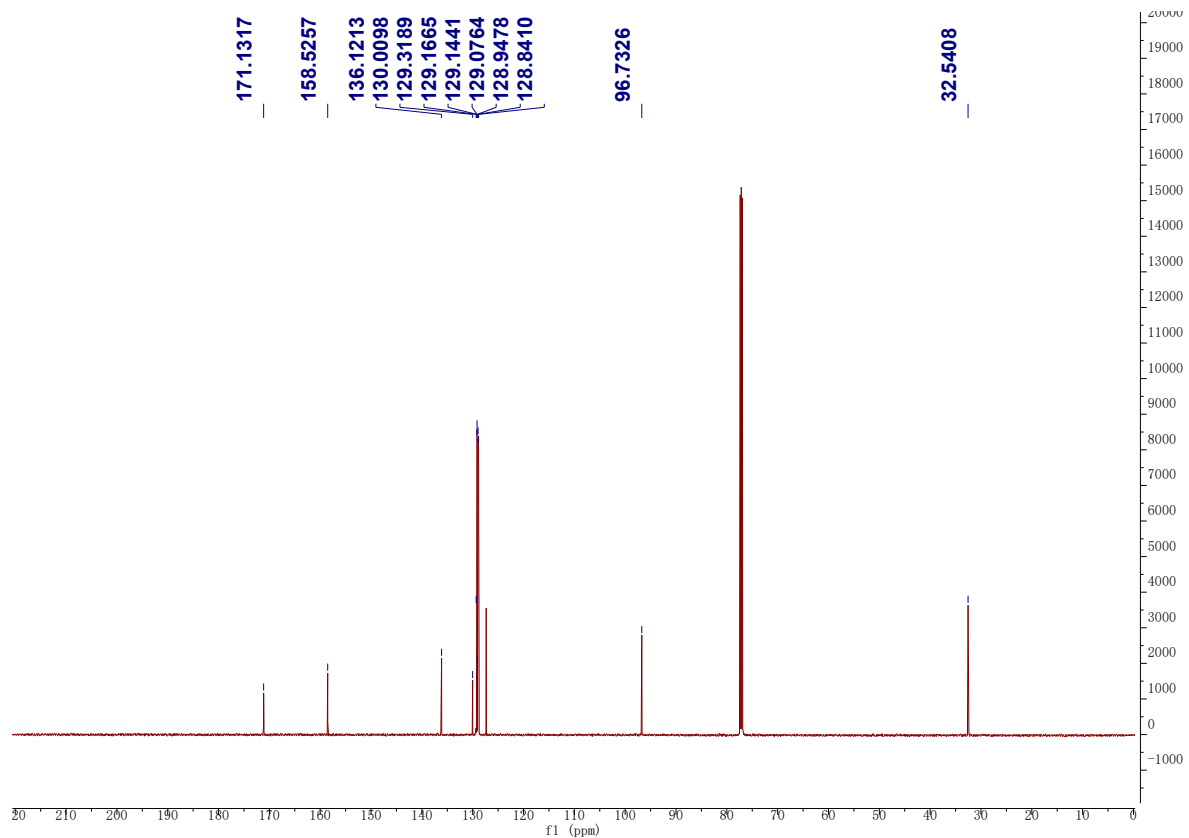
Supplementary Fig. 17 . Amount of PAM sites identified in the targetable window of *A. nidulans* genes (blue) and genes located in BGCs (red). Targetable window was defined as 400bp upstream of the start of the gene (TSS if available, otherwise -100bp of the start codon) or shorter if intergenic distance is less than 400bp. Even though LbCas12a has fewer targeting sites compared to Cas9, the median is 10 PAM sites per gene. In cases with limiting number of PAM sites, the use of the non-canonical site TTCN with the dLbCas12a^{D156R}-VPR variant could be explored, at the cost of losing efficiency for the canonical site, based on our observations at 37 °C (see Fig 4).

870



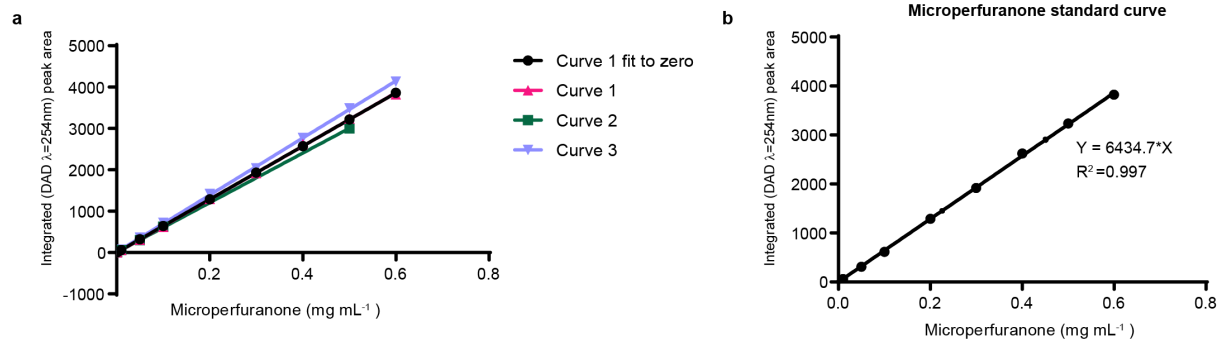
871
872
873

Supplementary Fig. 18 ¹H NMR spectrum (600 MHz) of microperfurane in CDCl₃-d.



874
875
876

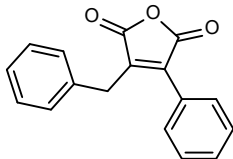
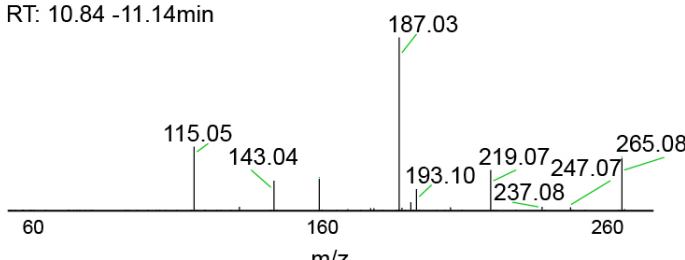
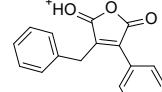
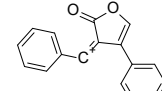
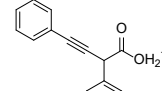
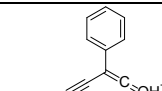
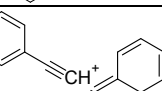
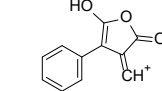
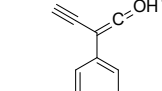
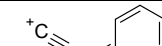
Supplementary Fig. 19 ¹³C NMR spectrum (150 MHz) of microperfurane in CDCl₃-d.



Supplementary Fig. 20. Calibration curve used for microperfurane quantification. **a.** Different calibration curves reproduce linearity but reflect the error from weighting microperfurane with the analytical balance. Individual values indicated as points. **b.** Curve 1 fit to zero was chosen as representative for quantification, points are the mean of three LC-DAD-MS injection technical replicates per point, SD is represented.

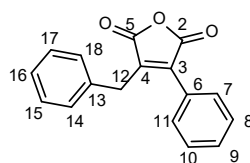
Supplementary Tables

Supplementary Table 1. Predicted spectra of dehydromicroperuranone based on CFM-ID⁴ is compared to LC-MS/MS (MS²) spectra of m/z 265 at different fragmentation events.

<div></div> <div>Dehydromicroperuranone</div>	<div>MS² m/z: 265.08 RT: 10.84 -11.14min</div> <div></div>				
Theoretical fragment m/z by CFM-ID ⁴	Observed m/z	Error (ppm)	Mass difference (Da)	Proposed structure by CFM-ID	
265.0859207	265.079	-26.1080659	0.0069207		
247.075356	247.0688	-26.53511896	0.006556		
237.0910061	237.0847	-26.598511	0.0063061		
219.0804414	219.0745	-27.12045446	0.0059414		
193.1011768	193.0959	-27.32735392	0.0052768		
187.0389705	187.0337	-28.17941366	0.0052705		
143.0491413	143.0451	-28.25192894	0.0040413		
115.0542266	115.0509	-28.91415886	0.0033266		

Supplementary Table 2. ¹H and ¹³C NMR data for dehydromicroperuranone (**2**) purified as peaks I-II and peak III showing identical chemical shifts in chloroform-*d* (Supplementary Fig. 9–12). a: overlapping peaks, or tentatively assigned based on prediction. The previously reported NMR chemical shifts for **2**⁵ are shown in the table for comparison.

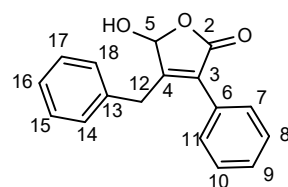
Carbon No.	2 in Chloroform- <i>d</i> Ref. ⁵		Peaks I-II in Chloroform- <i>d</i> This work		Peak III in Chloroform- <i>d</i> This work	
	¹³ C NMR	¹ H NMR	¹³ C NMR	¹ H NMR	¹³ C NMR	¹ H NMR
2	165.8 (s)	-	166.0 (s)	-	165.9 (s)	-
3	141.0 (s)	-	141.2 (s)	-	141.3 (s)	-
4	135.5 (s)	-	135.5 (s)	-	135.6 (s)	-
5	164.8 (s)	-	165.0 (d)	-	165.0 (s)	-
6	127.1 (s)	-	127.2 (s)	-	127.3 (s)	-
7	128.4 (d)	7.15 (5H, br s) ^a	129.23 (d)	7.21 (m) ^a	129.3 (d) ^a	7.21 (m) ^a
8	129.0 (d)	7.44 (5H, br s) ^a	129.17 (d)	7.63 (m) ^a	129.2 (d) ^a	7.63 (m) ^a
9	130.2 (d)	7.44 (5H, br s) ^a	131.3 (d)	7.55 (m) ^a	131.4 (s)	7.55 (m)
10	129.0 (d)	7.44 (5H, br s) ^a	129.17 (d)	7.63 (m) ^a	129.2 (d) ^a	7.63 (m) ^a
11	128.4 (d)	7.15 (5H, br s) ^a	129.23 (d)	7.21 (m) ^a	129.3 (d) ^a	7.21 (m) ^a
12	30.4 (t)	3.93 (2H, s)	30.6 (s)	4.03 (2H, s)	30.6 (s)	4.05 (2H, s)
13	140.6 (s)	-	140.8 (s)	-	140.8 (s)	-
14	129.3 (d)	7.15 (5H, br s) ^a	128.6 (d)	7.34 (m) ^a	128.6 (d)	7.34 (m)
15	129.0 (d)	7.44 (5H, br s) ^a	129.5 (d)	7.53 (m) ^a	129.5 (d) ^a	7.53 (m) ^a
16	127.3 (s)	7.15 (5H, br s) ^a	127.5 (d)	7.29 (m) ^a	127.5 (s)	7.28 (m)
17	129.0 (d)	7.44 (5H, br s) ^a	129.5 (d)	7.53 (m) ^a	129.5 (d) ^a	7.53 (m) ^a
18	129.3 (d)	7.15 (5H, br s) ^a	128.6 (d)	7.34 (m) ^a	128.6 (d)	7.34 (m)



Dehydromicroperuranone (**2**)

Supplementary Table 3. ^1H and ^{13}C NMR data for microperfuranone (**1**) in chloroform- d (supplementary Fig. 18–19). a: overlapping peaks, or tentatively assigned based on prediction. The previously reported NMR chemical shifts for **1**^{6,7} are shown in the table for comparison.

Carbon No.	1 in acetone- d_6 Ref. ⁶		1 in Chloroform- d Ref. ⁷		1 in Chloroform- d This work	
	^{13}C NMR	^1H NMR	^{13}C NMR	^1H NMR	^{13}C NMR	^1H NMR
2	170.9 (s)	-	171.6 (s)		171.1 (s)	-
3	130.8 (s)	-	129.7 (s)		130.0 (s)	-
4	159.6 (s)	-	158.9 (s)		158.5 (s)	
5	97.7 (d)	5.98 (br s)	97.2 (d)	5.89 (br s)	96.7 (d)	5.97 (br s)
5-OH	-	6.90 (br s)		N/A	-	N/A
6	130.2 (s)	-	129.1 (s)		129.1 (s)	-
7	129.9 (d)	7.54 (br d, 6.7)	129.0 (s)	N/A	129.2 (d)	7.57 (m) ^a
8	129.3 (d)	7.46 (m)	128.6 (d)	N/A	128.8 (d)	7.50 (m) ^a
9	129.6 (d)	7.43 (m)	128.9 (d)	N/A	128.9 (d)	7.52 (m) ^a
10	129.3 (d)	7.46 (m)	128.6 (d)	N/A	128.8 (d)	7.50 (m) ^a
11	129.9 (d)	7.54 (br d, 6.7)	129.0 (s)	N/A	129.2 (d)	7.57 (m) ^a
12	32.9 (t)	3.97 (2H, br s)	32.3 (s)	3.91 (2H, br s)	32.3 (s)	3.97 (2H, br s)
13	137.5 (s)	-	136.0 (s)		136.1 (s)	-
14	129.6 (d)	7.30 (m)	128.8 (d)	N/A	128.9 (d)	7.26 (m) ^a
15	129.7 (d)	7.26 (m)	128.9 (d)	N/A	129.1 (d)	7.34 (m) ^a
16	127.7 (d)	7.22 (m)	127.1 (d)	N/A	127.3 (d)	7.33 (m) ^a
17	129.7 (d)	7.26 (m)	128.9 (d)	N/A	129.1 (d)	7.34 (m) ^a
18	129.6 (d)	7.30 (m)	128.8 (d)		128.9 (d)	7.26 (m) ^a



Microperfuranone (**1**)

904

905 Additional Supplementary Tables 4-9 are found as tabs an Excel file:

906 Supplementary Table 4 : Strains used in this study

907 Supplementary Table 5 : Plasmids used in this study

908 Supplementary Table 6 : Protospacers targeted

909 Supplementary Table 7 : Oligonucleotides used to create crRNA/sgRNA

910 Supplementary Table 8 : Oligonucleotides

911 Supplementary Table 9 : Statistical Analysis

912

913 **Supplementary note 1 : Sequence of crRNA expression cassettes cloning sites**

914 **> Cloning site of *P_{gpdA}* *LbCas12a* crRNA cassette**

915 (**...**)**ATCTTCCCATCCAAGAACCTTTAATC**CAAGCTTATCGATACCGTCGACCTCGACTCTA
916 GAGGATCG**AATTTCTACTAAGTGTAGAT**GGAGACG**GAATTC**CGTCTCC**AATTTCTACT**
917 **AAGTGTAGAT**TATCTTCGAGGGGGGGCCCGGTACCGCCCCGTCCGGTCCTGCCCGTCA
918 CCGAGATCCACTTAACGTTACTGAAATCAT(**...**)

919 *A. nidulans* *P_{gpdA}* TSS(bold underlined) and *gpdA* 5'UTR (bold green underlined). *LbCas12a*
920 scaffold (blue italics). Bsmbl sites (underlined) .**EcoRI site (red)**. **TrpC Terminator (black**
921 **bold)**

922

923 **> Cloning site of *P_{U3}* *SpCas9* sgRNA cassette**

924 **TTAATTAA**(**...**)**CAAGTCAGAACATTTTGCTAACAGC**AGAGACG**GGCGCCGCTACAGGGC**
925 **GCGTCCCATTCGCCATTCAGGCTGCGCAACTGTTGGGAAGGGCGATCGGTGCGGGCC**
926 **TCTTCGCTATTACGCCAGCTGGCGAAAGGGGGATGTGCTGCAAGGCG****CGTCTCCGTTT**
927 **TAGAGCTAGAAATAGCAAGTTAAAATAAGGCTAGTCCGTTATCAACTTGAAAAAGTGGC**
928 **ACCGAGTCGGTGC****TTTTTTTTTCC****GCGGCGC**CTGCAGGTCGACCATA(**...**)

929 **PacI site (orange italics underlined)** *A. fumigatus* ***U3* promoter (bold green)**. *SpCas9*
930 ***sgRNA scaffold (blue italics)***. Bsmbl sites (underlined) .**LacZ fragment (red)**. Poly T
931 terminator (bold) . **NotI site (purple italics underlined)**

932

933 References

- 934 1. Sibthorp, C. *et al.* Transcriptome analysis of the filamentous fungus *Aspergillus*
935 *nidulans* directed to the global identification of promoters. *BMC Genomics* **14**, 847
936 (2013).
- 937 2. Yamano, T. *et al.* Crystal Structure of Cpf1 in Complex with Guide RNA and Target
938 DNA. *Cell* **165**, 949–962 (2016).
- 939 3. Yamano, T. *et al.* Structural Basis for the Canonical and Non-canonical PAM

- Recognition by CRISPR-Cpf1. *Mol. Cell* **67**, 633–645.e3 (2017).
4. Allen, F., Pon, A., Wilson, M., Greiner, R. & Wishart, D. CFM-ID: A web server for annotation, spectrum prediction and metabolite identification from tandem mass spectra. *Nucleic Acids Res.* **42**, (2014).
5. Hamasaki, T., Nakajima, H., Yokota, T. & Kimura, Y. A New Metabolite, 3-Carboxy-2,4-diphenyl-but-2-enoic Anhydride, Produced by *Aspergillus nidulans*. *Agric. Biol. Chem.* **47**, 891–892 (1983).
6. Fujimoto, H., Asai, T., Kim, Y. P. & Ishibashi, M. Nine constituents including six xanthone-related compounds isolated from two ascomycetes, *Gelasinospora santi-florii* and *Emericella quadrilineata*, found in a screening study focused on immunomodulatory activity. *Chem. Pharm. Bull.* **54**, 550–553 (2006).
7. Yeh, H. H. *et al.* Molecular genetic analysis reveals that a nonribosomal peptide synthetase-like (NRPS-like) gene in *Aspergillus nidulans* is responsible for microperfuranone biosynthesis. *Appl. Microbiol. Biotechnol.* **96**, 739–748 (2012).